Ten years of GOME/ERS-2 total ozone data—The new GOME data processor (GDP) version 4: 1. Algorithm description

M. Van Roozendael,[1] D. Loyola,[2] R. Spurr,[3] D. Balis,[4] J.-C. Lambert,[1] Y. Livschitz,[2] P. Valks,[2] T. Ruppert,[5] P. Kenter,[6] C. Fayt,[1] and C. Zehner[7]

Received 15 June 2005; revised 17 January 2006; accepted 27 March 2006; published 26 July 2006.

[1] The Global Ozone Monitoring Instrument (GOME) was launched on European Space Agency's ERS-2 platform in April 1995. The GOME data processor (GDP) operational retrieval algorithm has generated total ozone columns since July 1995. In 2004 the GDP system was given a major upgrade to version 4.0, a new validation was performed, and the 10-year GOME level 1 data record was reprocessed. In two papers, we describe the GDP 4.0 retrieval algorithm and present an error budget and sensitivity analysis (paper 1) and validation of the GDP total ozone product and the overall accuracy of the entire GOME ozone record (paper 2). GDP 4.0 uses an optimized differential optical absorption spectroscopy (DOAS) algorithm, with air mass factor (AMF) conversions calculated using the radiative transfer code linearized discrete ordinate radiative transfer (LIDORT). AMF computation is based on the TOMS version 8 ozone profile climatology, classified by total column, and AMFs are adjusted iteratively to reflect the DOAS slant column result. GDP 4.0 has improved wavelength calibration and reference spectra and includes a new molecular Ring correction to deal with distortion of ozone absorption features due to inelastic rotational Raman scattering effects. Preprocessing for cloud parameter estimation in GDP 4.0 is done using two new cloud correction algorithms: OCRA and ROCINN. For clear and cloudy scenes the precision of the ozone column product is better than 2.4 and 3.3%, respectively, for solar zenith angles up to 80°. Comparisons with ground-based data are generally at the 1–1.5% level or better for all regions outside the poles.

Citation: Van Roozendael, M., et al. (2006), Ten years of GOME/ERS-2 total ozone data—The new GOME data processor (GDP) version 4: 1. Algorithm description, *J. Geophys. Res.*, *111*, D14311, doi:10.1029/2005JD006375.

1. Introduction and Overview

1.1. Background and Motivation

[2] Accurate global ozone records from passive remote sensing observations play a vital role in ozone trend analysis and climate change studies. Long-term global monitoring of total ozone from satellite-borne UV spectrometers is currently in a transitional phase. The Global Ozone Monitoring Experiment (GOME) [*Burrows et al.*, 1999a] was launched on board the Second European Remote Sensing Satellite (ERS-2) in April 1995. GOME has been operational since July 1995, but spatial coverage has been limited since July 2003 due to problems with tape storage on ERS-2. Also, GOME level 1 data quality has deteriorated considerably in the last two years, mainly due to instrument degradation. SCIAMACHY [*Bovensmann et al.*, 1999] was launched in March 2002 on board the ENVISAT platform and is currently operational. EUMETSAT's new generation ozone instrument is GOME-2: three identical instruments are planned, with the first scheduled for launch in spring 2006 on the first METOP satellite.

[3] The Total Ozone Monitoring Spectrometer (TOMS) total ozone record at NASA dates back to 1978, and there is no successor mission with a new TOMS instrument planned. The latest algorithm for TOMS is version 8 (P. K. Bhartia, Algorithm theoretical baseline document, TOMS v8 total ozone algorithm, available at http://toms.gsfc.nasa.gov/version8/version8_update.html). The current record with Earth Probe (EP) TOMS shows an instrumental drift after 2001 due to scan mirror degradation; TOMS data after that time are not recommended to be used for trend analysis. The SBUV total ozone record at NOAA dates back to 1970 with the last SBUV/2 instrument still

[1]Belgian Institute for Space Aeronomy, Brussels, Belgium.
[2]Remote Sensing Technology Institute, German Aerospace Center, Wessling, Germany.
[3]RT Solutions, Inc., Cambridge, Massachusetts, USA.
[4]Laboratory of Atmospheric Physics, Department of Physics, Aristotle University of Thessaloniki, Thessaloniki, Greece.
[5]German Remote Sensing Data Center, German Aerospace Center, Wessling, Germany.
[6]Science & Technology BV, Delft, Netherlands.
[7]European Space Research Institute, European Space Agency, Frascati, Italy.

0148-0227/06/2005JD006375

operational. NASA's current instrument is the Ozone Monitoring Instrument (OMI) spectrometer [*Stammes et al.*, 1999], on the EOS Aura platform launched in mid-July 2004. OMI is regarded the successor mission to the TOMS series. NASA and NOAA's new generation ozone instrument is the Ozone Mapping and Profiler Suite (OMPS); the first of these is scheduled for launch no earlier than 2008 on the NPOESS Preparatory Project (NPP) satellite.

[4] Ozone trend analysis requires a long-term, accurate and stable data record (typically, the ability to measure a 1% change in total ozone concentrations globally over a period of about 10 years). With the long-term stability of GOME, and the absence of instrumental drift in the ozone record over the lifetime of the mission, GOME is a good candidate for this analysis. Although the ozone record generated from versions of GDP up to 3.0 could be considered for trend analysis as far as the stability of the record is concerned, what really makes the difference with the GDP 4.0 ozone record is the much reduced sensitivity to atmospheric parameters; in other words, the lack of "atmospheric drifts" interfering with the targeted total ozone trend. As we will see in particular in the sequel paper on GDP validation, the upgrade from GDP 3.0 to GDP 4.0 has ensured that the accuracy of the GOME total ozone record is now on a par with that for TOMS Version 8. The combined use of both TOMS and GOME data records can now be envisaged for ozone trend analysis.

[5] In summer 2002, the European Space Agency (ESA) made a call for improved total ozone algorithms to meet this accuracy requirement. From this call, three new algorithms were developed for GOME application in 2003 and subsequently used to reprocess the GOME total ozone record. These algorithms are all based on the differential optical absorption spectroscopy (DOAS) technique. They are (1) the WFDOAS algorithm [*Coldewey-Egbers et al.*, 2005; *Weber et al.*, 2005], (2) the TOGOMI/TOSOMI algorithm [*Eskes et al.*, 2005], and (3) the GDOAS algorithm (this work). GDOAS was selected in early 2004 for implementation in the German Processing and Archiving Facility (D-PAF) at the German Aerospace Center (DLR) as part of a major operational upgrade to version 4.0 of the GOME data processor (GDP). GDP 4.0 has become part of the ESA ERS Ground Segment in 2004.

[6] We report the GDP 4.0 upgrade and product validation in two successive papers. This paper contains a description of the GDP 4.0 GDOAS algorithm and its implementation in the GDP environment. The second paper [*Balis et al.*, 2006] deals with the external geophysical validation of the GOME total ozone product. Although the emphasis in these two papers is on the total ozone product, reprocessing has also been completed for the GOME total NO_2 data record.

1.2. GOME Instrument

[7] ERS-2 is a Sun-synchronous polar orbiting satellite, with a period of about 100 min and a local equator crossing time of 10.30h. GOME is an across-track nadir-viewing spectrometer; in normal viewing mode, it has three forward scans followed by a back scan. Each forward scan has a footprint size of 320×40 km^2 for a 1.5-s detector readout integration time. The maximum swath is 960 km, with nominal scan angle $\pm 31^\circ$ at the spacecraft, so that global coverage is achieved at the equator within three days. There is also a static polar viewing mode for improved sounding of polar latitudes during springtime. GOME has 3584 spectral channels distributed over four serial readout detectors; the wavelength range is 240 to 793 nm, with a moderate spectral resolution of 0.2 to 0.4 nm. GOME also has a Pt-Ne-Cr lamp for in-flight wavelength calibration and a diffuser plate for the daily determination of solar irradiance. GOME has also three broadband (>100 nm) Polarization Measurement Devices (PMDs) measuring light in a direction parallel to the slit (PMDs have a footprint size of 20×40 km^2). The PMDs' main purpose is to generate a polarization correction for the level 1 spectra (calibrated and geolocated radiances), but they are also used for cloud detection. More details on the GOME instrument are given by *Burrows et al.* [1999a, appendix] and in the GOME users' manual [*Bednarz*, 1995].

[8] The moderate spectral resolution of GOME resolves absorption signatures of chemically important atmospheric trace gases. Ozone is the principal target species. In addition to total ozone, a number of global ozone profile retrievals have been made [see, e.g., *Munro et al.*, 1998; *Hoogen et al.*, 1999; *Hasekamp and Landgraf*, 2001; *van der A et al.*, 2002; *Müller et al.*, 2003; *Liu et al.*, 2005]. The instrument also retrieves total columns of a number of minor trace species including NO_2 [see, e.g., *Martin et al.*, 2002], HCHO [see, e.g., *Thomas et al.*, 1998; *Chance et al.*, 2000], BrO [e.g., *Chance*, 1998], SO_2 [e.g., *Thomas et al.*, 2005], and the total H_2O vapor content [e.g., *Wagner et al.*, 2003]. Other products include cloud parameter information [e.g., *Koelemeijer et al.*, 2001] and absorbing aerosol index [e.g., *De Graaf et al.*, 2005]. For an overview of mission targets, see *Burrows et al.* [1999a]. The GOME data processor (GDP) has been operational since August 1996 following the GOME commissioning phase [*Loyola et al.*, 1997]. The main operational level 2 products from GDP are global distributions of total column O_3 and NO_2. The entire O_3 and NO_2 data records since July 1995 have now been reprocessed following upgrades (GDP level 1-to-2 versions 2.0, 2.7, 3.0 and now 4.0) to the original retrieval algorithm.

1.3. Overview of the GDP 4.0 Algorithm

[9] As its name implies, GDOAS is a classical DOAS-AMF fitting algorithm for the generation of total column amounts. The algorithm has two major steps: a DOAS least squares fitting for the effective slant column of ozone, followed by the computation of a suitable air mass factor to make the conversion to the vertical column density. Figure 1 is a schematic flowchart for the GDP 4.0 total ozone algorithm. In a preprocessing step, cloud information (fractional cover, cloud top height and cloud albedo) is derived before the above two major algorithm components are executed. In GDP 4.0 cloud algorithm products are computed directly by calls to the OCRA/ROCINN algorithms [*Loyola and Ruppert*, 1998; *Loyola*, 2004].

[10] The first major algorithm component is the DOAS fitting. This is a straightforward least squares inversion to deliver the effective slant column of total ozone, plus a number of auxiliary fitted parameters and error diagnostics. The latter include an effective temperature for the ozone absorption, a slant column for NO_2 (regarded as an inter-

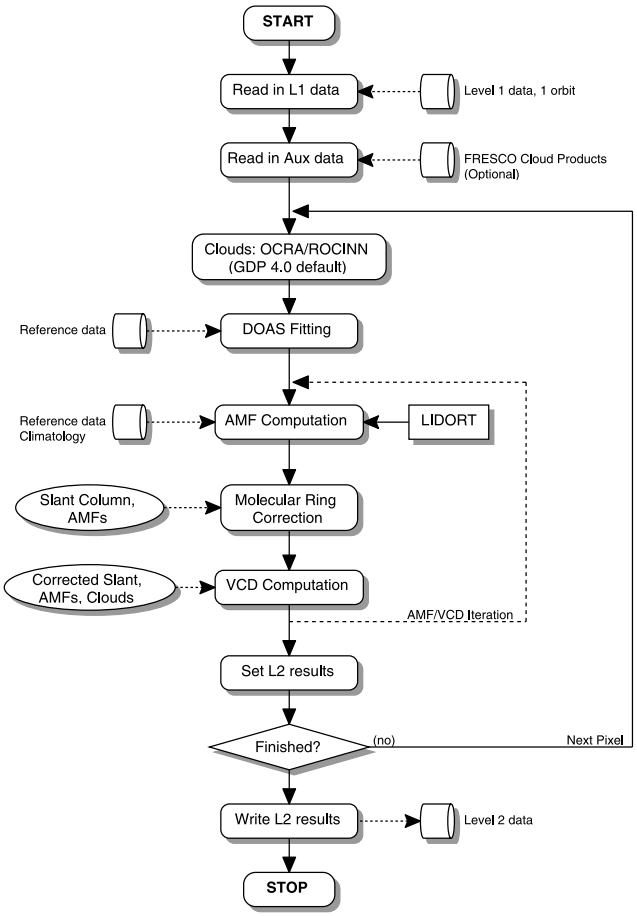

Figure 1. Flow diagram for the GDP 4.0 algorithm.

fering species in the ozone UV window), wavelength registration parameters for resampling the earthshine spectrum, scaling factors for interference due to undersampling and Ring effects, and low-pass filter closure parameters.

[11] The second major component is the iterative air mass factor/vertical column density (AMF/VCD) computation to generate the final vertical column. An initial guess is made for the VCD. At each iteration step, ozone air mass factors (to ground level and to cloud top) are computed for the current guess of the vertical column. This radiative transfer calculation uses a column-classified ozone profile climatology. Then the DOAS slant column is adjusted using the molecular Ring correction (to compensate for interference effects in ozone absorption features due to inelastic rotational Raman scattering). This adjusted slant column is then used in conjunction with preprocessed cloud information and the AMF values to update the VCD guess. The pixel processing is completed with an assignation of the level 2 output (total column, errors and retrieval diagnostics, and auxiliary output such as surface pressure and selected level 1 geolocation information) for one orbit of data.

[12] The GDP 4.0 algorithm components are described in the next four chapters, starting with the DOAS fitting (section 2), moving on to the iterative AMF/VCD computation (section 3), the molecular Ring correction (section 4) and the cloud preprocessing (section 5). In section 6 we present an error budget for the total ozone algorithm, and discuss a number of sensitivity tests.

[13] Some of the material referenced in this paper is not readily available, so we have included a number of reports and papers on the Web (http://wdc.dlr.de/sensors/gome/gdp4.html) under the rubric "Technical Documentation."

1.4. Summary of Changes From GDP 3.0 to GDP 4.0

[14] In this section we summarize the main changes between the previous version GDP 3.0 and the present upgrade to version 4.0. These changes are conveniently displayed in Table 1. Details of the GDP 3.0 algorithm may be found in a recent publication [*Spurr et al.*, 2005].

[15] For total ozone, all GDP versions have used a single contiguous fitting window from 325 nm to 335 nm covering part of the O_3 Huggins bands absorption features. NO_2 DOAS fitting in all versions has used the visible window 425 nm to 450 nm. Initial GDP algorithms used cross sections from literature (for example, *Bass and Paur* [1985] for O_3), but in GDP 3.0 and GDP 4.0, the GOME-measured flight model cross sections for O_3 [*Burrows et al.*, 1999b] and NO_2 [*Burrows et al.*, 1998] were implemented. Both GDP 3.0 and 4.0 use two O_3 reference cross sections to retrieve the effective temperature in addition to ozone slant column [*Richter and Burrows*, 2002]. Both GDP versions use O_3 and NO_2 cross sections resampled with an initial wavelength shift. In GDP 3.0, explicit shift and squeeze fitting for wavelength registration was done only for the orbital solar spectrum resampled to earthshine

Table 1. Summary of Algorithm Changes from GDP 3.0 to 4.0

Algorithm	Feature	GDP 3.0 Implementation	GDP 4.0 Implementation
DOAS	cross sections preshift	0.012 nm	0.016 nm
DOAS	shift reference	level 1b earthshine spectrum	level 1b solar spectrum
DOAS	wavelength registration	—	additional cross correlation applied
AMF/VCD	AMF computation	look-up table plus neural network parameterization	direct calculation using LIDORT
AMF/VCD	ozone profile climatology	from TOMS V7 algorithm	from TOMS V8 algorithm
AMF/VCD	surface albedo	External data	GOME/TOMS LER data set
AMF/VCD	wavelength for calculation	325.0 nm	325.5 nm
AMF/VCD	adjustment of slant column using molecular Ring	—	new implementation
RING	molecular Ring correction	—	new implementation
CLOUD	cloud fraction	ICFA fitted	OCRA derived
CLOUD	cloud top height	ISCCP Climatology	ROCINN fitted
CLOUD	cloud top albedo	Fixed at 0.8	ROCINN fitted

wavelength grids. In GDP 4.0, level 1b wavelength calibration has been improved by matching the wavelength grid of the GOME solar spectrum to some solar reference data (see section 2.1). During the DOAS fitting the GOME earthshine spectra is then resampled to the new wavelength grid of the solar data.

[16] An undersampling correction was introduced in GDP 3.0 to compensate for GOME's sampling slightly below the Nyquist criterion [*Slijkhuis et al.*, 1999]. This is present also in GDP 4.0, and the reference undersampling spectrum has been recalculated. Both GDP 3.0 and GDP 4.0 use a Ring reference spectrum derived from convolution of Raman cross sections with a high-resolution solar spectrum [*Chance and Spurr*, 1997]. The Ring effect filling of ozone absorption features was not treated in GDP 3.0. In the version 4.0 upgrade, a new *Molecular Ring correction* has been implemented. This is arguably the most important improvement from GDP 3.0 to GDP 4.0. It is worth noting that the telluric Ring effect contribution has also been addressed in the other two algorithms used for GOME total ozone reprocessing [*Coldewey-Egbers et al.*, 2005; *Eskes et al.*, 2005], and we return to this in detail in section 4.

[17] The iterative AMF/VCD technique was first introduced by *Spurr* [1999] [see also *Marquard et al.*, 2000] and was subsequently used in the GDP 3.0 operational environment [*Spurr et al.*, 2005]. The method is also used in GDP 4.0 but there are significant differences. In GDP 3.0, look-up tables of O_3 AMFs were prepared using the LIDORT radiative transfer model [*Spurr et al.*, 2001; *Spurr*, 2002], and the LUTs were then used to train neural network ensembles for fast computation of AMFs [*Loyola*, 1999]. In GDP 4.0, AMFs are calculated *directly* using the LIDORT radiative transfer model and the single AMF is now calculated at 325.5 nm (replacing the 325.0 nm value chosen for GDP 3.0). In GDP 3.0, AMFs were based on the TOMS Version 7 O_3 profile climatology [*Wellemeyer et al.*, 1997], while GDP 4.0 AMFs are based on O_3 profile data as used in the TOMS Version 8 algorithm (http://toms.gsfc.nasa.gov/version8/version8_update.html). For surface albedos, GDP 4.0 uses a new data set based on surface reflectances derived from GOME data [*Koelemeijer et al.*, 2003] and TOMS data [*Herman and Celarier*, 1997]. Finally, the new molecular Ring correction in GDP 4.0 depends on the AMF, and therefore the AMF/VCD computation must include this correction to the fitted effective slant column at each iteration step. In GDP 3.0, NO_2 AMFs were determined by means of a single scatter computation followed by a multiple scatter correction from a look-up table [*Spurr et al.*, 2005]. In GDP 4.0, NO_2 AMFs are calculated directly using the LIDORT radiative transfer code.

[18] In GDP 3.0, fractional cloud coverage was retrieved from the initial cloud-fitting algorithm (ICFA) [*Kuze and Chance*, 1994]. Cloud top pressure was supplied from the international satellite cloud climatology project (ISCCP) database [*Schiffer and Rossow*, 1983], and a fixed cloud top albedo of 0.8 was assumed. In complete contrast, GDP 4.0 generates cloud information (cloud top height and albedo, effective cloud fraction) from two new cloud algorithms (OCRA and ROCINN [*Loyola*, 2000, 2004]) installed as part of the GDP operating system.

[19] Following earlier validation campaigns in 1996 [see, e.g., *Lambert et al.*, 1996] and 1998/1999 [*Lambert et al.*, 1999, 2000], a major ESA-sponsored sensitivity study [*Van Roozendael et al.*, 2002] and validation [*Lambert et al.*, 2002] was performed in 2002 on the operational GDP 3.0 total ozone algorithm. A number of improvements to GDP 3.0 were suggested and most of these have now been implemented in the GDOAS algorithm as part of the operational GDP 4.0 system.

1.5. Operational GDP 4.0 Environment

[20] GDP 4.0 is part of a new system environment. This is universal processor for UV/VIS atmospheric spectrometers (UPAS) [*Livschitz and Loyola*, 2003]: a new generation level 2 system for the processing of operational near real time and off-line trace gas retrieval products. UPAS takes as input the calibrated and geolocated level 1 radiances from different sensors (e.g., GOME on ERS-2 and GOME-2 on METOP) and produces total columns of trace gases such as O_3, NO_2, BrO, SO_2, HCHO and OClO. From the computational performance viewpoint, the major new feature in GDP 4.0 is the calculation of AMFs using explicit calls to the LIDORT radiative transfer model. The average GDP 4.0 processing time includes ~15% on preprocessing tasks (includes OCRA/ROCINN), ~15% on DOAS, ~60% on LIDORT AMF calculations, and the rest on level 1 loading and other tasks. The UPAS system is based on client/server architecture, and this makes it possible to run the system with an unlimited number of processing nodes. The GDP 4.0 operational reprocessing system is based on 10 Linux PCs, each with 2 processors (3 GHz CPUs). The reprocessing of the complete 10-year GOME data record can be done in just 10 days.

2. DOAS Algorithm In GDP 4.0

2.1. DOAS Slant Column Fitting

[21] A detailed treatment of the GOME DOAS application may be found in the GDP 3.0 paper [*Spurr et al.*, 2005]; here we summarize the main points and focus on improvements in GDP 4.0. In DOAS fitting, the basic model is the Beer-Lambert extinction law for trace gas absorbers. An external polynomial closure term accounts for broadband effects: molecular scattering, aerosol scattering and absorption and reflection from the Earth's surface. We also include additive spectra for Ring effect interference and for undersampling. The fitting model is then

$$Y(\lambda) \equiv \ln\left[\frac{I_\lambda(\Theta)}{I^0_\lambda(\Theta)}\right] = -\sum_g E_g(\Theta)\sigma_g(\lambda) - \sum_{j=0}^{3} \alpha_j \left(\lambda - \lambda^*\right)^j - \alpha_R R(\lambda) - \alpha_U U(\lambda) \quad (1)$$

Here, I_λ is the earthshine spectrum at wavelength λ, I^0_λ the solar spectrum, $E_g(\Theta)$ the effective slant column density of gas g along geometrical path Θ, $\sigma_g(\lambda)$ is the associated trace gas absorption cross section. The second term in equation (1) is the closure polynomial (a cubic filter has been assumed), with λ^* a reference wavelength for this polynomial. The last two terms on the right hand side of equation (1) are the additive terms for the Ring reference spectrum $R(\lambda)$ and the undersampling spectrum $U(\lambda)$. The fitting minimizes the weighted least squares difference

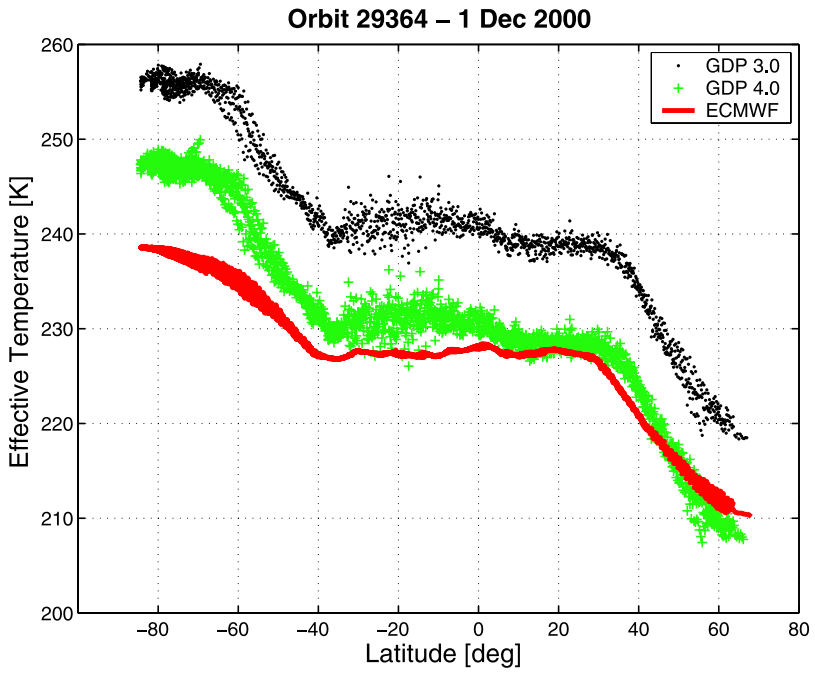

Figure 2. Retrieved effective temperature for O_3 cross sections derived from GDP V3.0 (dots) and GDP V4.0 (green crosses) and compared with ECMWF analysis data (solid red lines) for one GOME orbit from 1 December 2000.

between measured and simulated optical densities $Y_{meas}(\lambda)$ and $Y_{sim}(\lambda)$ respectively. The model in equation (1) is linear in the slant columns $E_g(\Omega)$, the polynomial coefficients $\{\alpha_k\}$ and the Ring and undersampling scaling parameters α_R and α_U.

[22] Shift and squeeze parameters may be applied to cross-section wavelength grids to improve wavelength registration against level 1 data. Experience with DOAS in the operational GDP processor has shown that fitting of such nonlinear parameters on a pixel-by-pixel basis can sometimes leads to numerical instability. In GDP 4.0, trace gas cross sections have been resampled based on a shift of +0.016 nm (toward longer wavelengths) before use in the operational processing (no squeeze has been applied). Finally, the solar and earthshine spectra in the left hand side of equation (1) must be registered on a common wavelength grid. In GDP 4.0, the solar spectrum is the reference, and the earthshine data is always resampled by means of a fitted wavelength shift and squeeze. Resampling issues are discussed in more detail below.

[23] Before GDP 3.0, temperature dependence in the ozone Huggins bands was specified through a single effective temperature T_{eff} chosen externally from climatology. It was found that DOAS fitting for GOME total ozone achieves greater accuracy when two ozone cross sections at different temperatures are used as reference spectra [*Richter and Burrows*, 2002]. The effective temperature T_{eff} is then retrieved in addition to the slant column. It has been shown that the DOAS root mean squares of spectral residuals are lowered by a factor of 2 [see, e.g., *Spurr et al.*, 2005, Figure 1], and total ozone results agree better with validation data [*Lambert et al.*, 2002]. In GDP 3.0, a positive bias of 10–20 K (depending on orbit) was observed in T_{eff}; when compared with values derived from temperature profiles extracted from meteorological data. The improved wavelength registration in GDP 4.0 (see next section) has largely removed this bias. This can be seen in Figure 2, where we compare effective ozone temperatures derived from GDP 3.0 and 4.0 with those derived from ECMWF analysis data. In the latter case, effective temperatures have been calculated from a weighted average of the ECMWF profile data, using as weights the calculated partial slant column of ozone in each atmospheric layer.

2.2. Reference Spectra and Resampling Issues

[24] GDP 3.0 and 4.0 use the latest released version of the GOME Flight Model cross sections (O_3 and NO_2), the so-called GOME FM98 data [*Burrows et al.*, 1998, 1999b]. For GDP 3.0, cross sections were preshifted by +0.012 nm. Preshifting of ozone cross sections is required to compensate for inaccuracies in the wavelength calibration of the GOME FM98 data [*Burrows et al.*, 1999b]. Following a recommendation from the GDP 3.0 geophysical validation campaign [*Van Roozendael et al.*, 2002], O_3 cross sections are now corrected for the so-called solar I_0 effect [*Aliwell et al.*, 2002], and have been implemented in GDP 4.0 with a preshift of +0.016 nm. This value was determined from a series of test retrievals in which the ozone cross-section shift was optimized as part of the DOAS procedure itself (see Figure 3). The same value applies to NO_2 cross sections (this trace gas is an interfering species in the ozone window, and an associated slant column amplitude is included in the DOAS fitting). This change in preshift value has removed a systematic positive bias of 1.5% in GDP 3.0 total ozone, and as noted above, it has largely removed the effective temperature bias.

[25] In GDP 4.0, the solar spectrum is used as the wavelength reference. Shift and squeeze parameters are

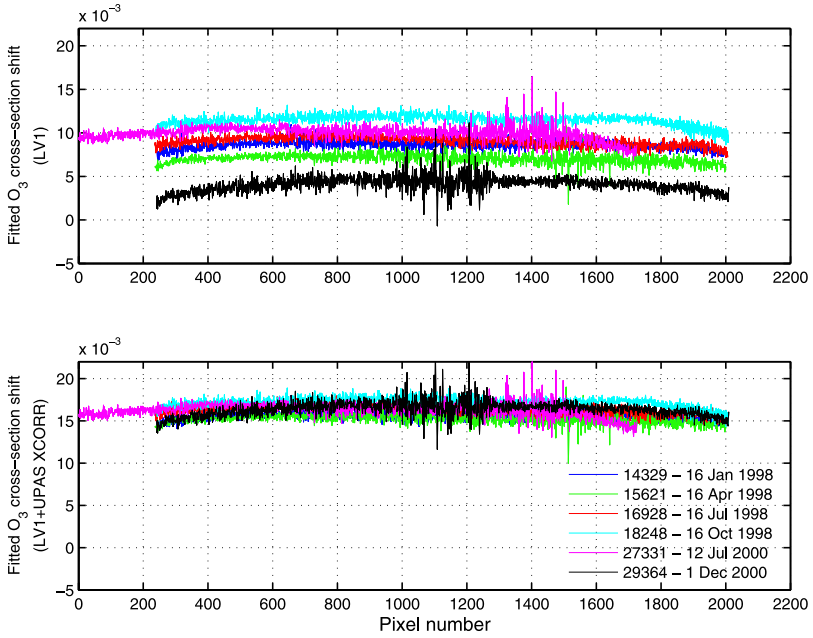

Figure 3. Improvement in fitted ozone cross section wavelength shifts resulting from an additional post-level 1 wavelength cross correlation. (top) Fitted shifts derived using the original extracted level 1 data; (bottom) fitted shifts determined after the additional wavelength cross correlation ("UPAS XCORR") applied to level 1 data. Results are shown for six orbits, as indicated in the legend; the x coordinate denotes orbit pixel numbers.

applied to each Earthshine wavelength grid in order to resample the Earthshine spectrum. The GOME earthshine and solar spectra are produced by the GDP level 0-to-1 algorithm by means of the level 0-to-1b extractor [*Aberle et al.*, 2002; *Slijkhuis et al.*, 2004]. To improve the wavelength calibration of the level 1 spectra, we apply window-dependent preshifts to parts of the solar spectrum before each orbit of data is processed. These preshifts are established by cross correlation with a high-resolution solar spectrum [*Chance and Spurr*, 1997] over limited wavelength ranges covering the main fitting windows (325–335 nm for O_3, 425–450 nm for NO_2 in the visible, and 758–772 nm covering the O_2 A band as used in the ROCINN algorithm). Figure 3 demonstrates the improved stability in O_3 fitting due to this calibration enhancement (which has been called "post-level 1 processing"). Figure 3 (top) shows fitted cross-section shifts using the original level 1 wavelength calibration, while Figure 3 (bottom) shows the same quantities processed with level 1 data that includes the additional wavelength registration (indicated by "UPAS-XCORR" in the y axis label). The impact of the shift on the ozone column is about 2.5% per 0.01 nm shift error. Hence inaccuracies of the GOME wavelength calibration of the order 0.008 nm as shown in Figure 3 (top) directly translate into errors on total ozone of the order of 2%.

[26] The Ring effect (filling-in of well-modulated solar and absorption features in earthshine spectra) is due to inelastic rotational Raman scattering (RRS). In DOAS fitting, it is treated as an additional absorber, by means of an additive Ring reference spectrum and associated scaling parameter, as in equation (1). The simplest "Fraunhofer" Ring spectrum is obtained by folding rotational Raman cross sections at a fixed temperature with a high-resolution Fraunhofer spectrum taken from the Kitt Peak Observatory [*Chance and Spurr*, 1997], but this does not include a telluric contribution. In the UV window 325–335 nm, Ring effect distortion of O_3 Huggins bands absorption features is large enough to seriously compromise total ozone fitting accuracy. As noted already, a new molecular Ring effect correction was developed for GOME total ozone in GDP 4.0. This correction is an ex post facto scaling of the DOAS slant column result, and it is performed at each iteration step in the AMF/VCD calculations (see section 3). A description of this molecular Ring correction algorithm is presented in section 4.

[27] The DOAS state vector for linear fitting in GDP 4.0 has nine parameters: two effective slant columns [DU] of O_3 and NO_2, one fitting parameter for a second O_3 cross section (to derive the effective temperature T_{eff}), four closure coefficients, and two additive scaling factors (corresponding to Fraunhofer Ring and undersampling reference spectra). There are two parameters in the nonlinear least squares fitting: a wavelength shift and squeeze for resampling the earthshine spectrum on to the solar spectrum reference wavelength grid.

3. AMF/VCD Computations in GDP 4.0

3.1. Iterative AMF/VCD Method

[28] The ozone AMF definition that has been used in all GDP versions is the traditional one:

$$A = \frac{\log(I_{nog}/I_g)}{\tau_{vert}}, \tag{2}$$

where I_g is the radiance for an atmosphere including ozone as an absorber, I_{nog} is the radiance for an ozone-free

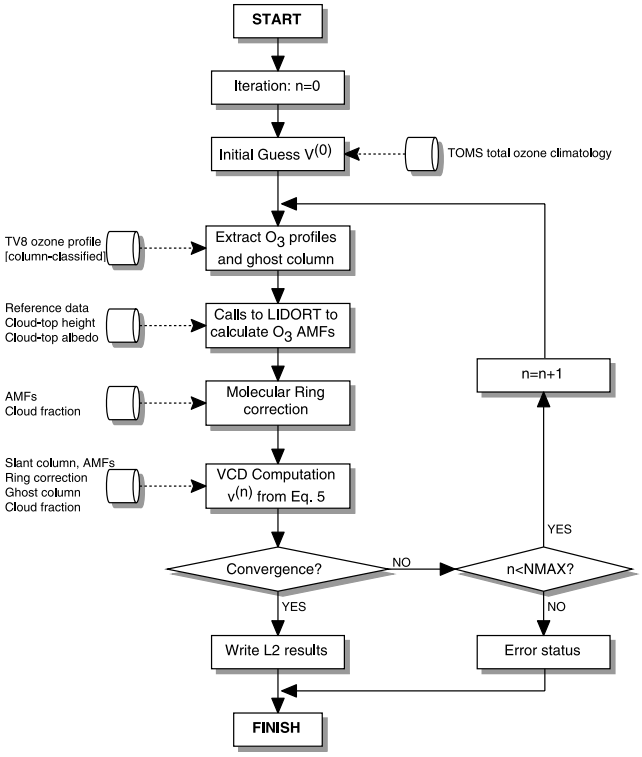

Figure 4. Functional diagram of the iterative solution scheme for O_3 air mass factors and vertical column densities.

atmosphere and τ_{vert} is the vertical optical thickness of ozone. For GOME scenarios, computation of the vertical column density (VCD) has always proceeded via the relation:

$$V = \frac{E + \Phi G A_{cloud}}{(1-\Phi)A_{clear} + \Phi A_{cloud}}, \tag{3}$$

where E is the DOAS-retrieved slant column, A_{clear} the clear sky AMF, A_{cloud} the AMF for the atmosphere down to the cloud top level, and the "ghost column" G is the quantity of ozone below the cloud top height. This formula assumes the independent pixel approximation for cloud treatment. In GDP 3.0, Φ is the fractional cloud cover c_f. In GDP 4.0, we use the "intensity-weighted cloud fraction" Φ, defined as

$$\Phi = \frac{c_f I_{cloud}}{(1-c_f)I_{clear} + c_f I_{cloud}}, \tag{4}$$

where I_{clear} and I_{cloud} are the backscattered radiances for cloud-free and cloud-covered scenes respectively. I_{clear} and I_{cloud} are calculated with the LIDORT radiative transfer model, and depend mainly on the surface and cloud albedos and on the GOME viewing geometry.

[29] AMFs depend on ozone profiles through the radiative transfer model. In traditional DOAS retrievals, the ozone AMF depends on a fixed ozone profile taken from climatology; one application of equation (3) yields the VCD. In the iterative approach to AMF calculation, we use a column-classified ozone profile climatology to establish a unique relationship between the ozone profile and its corresponding total column amount. The AMF values are now considered to be functions of the VCD through this profile-column relation, and the above formula in equation (3) is used to update the VCD value according to

$$V^{(n+1)} = \frac{E + \Phi G^{(n)} A^{(n)}_{cloud}}{(1-\Phi)A^{(n)}_{clear} + \Phi A^{(n)}_{cloud}} \tag{5}$$

Here the (n) superscript indicates the iteration number. The AMFs $A^{(n)}_{clear}$ and $A^{(n)}_{cloud}$, and the ghost column $G^{(n)}$, depend on the value of VCD $V^{(n)}$ at the nth iteration step. In this iteration, the slant column E reflects the true state of the atmosphere and acts as a constraint on the iteration. Equation (5) is applied repeatedly until the relative change in $V^{(n)}$ is less than a prescribed small number ε. In other words, convergence is reached when $|(V_{n+1}/V_n) - 1| < \varepsilon$. For a value of ε set at 10^{-4} (the GDP 4.0 operational baseline), convergence is rapid and three to five iterations are usually sufficient. The first guess choice V_0 comes from a zonally averaged total column climatology derived from many years of TOMS data.

[30] In GDP 4.0, there is now a molecular Ring correction M applied to the slant column E, and we must therefore use a corrected slant column $E_{\mathrm{corr}} = E/M$ in the iteration. As we will see in section 4, M depends on the total AMF, defined to be $A_{total} = (1-\Phi)A_{clear} + \Phi A_{cloud}$. Clearly M will need to be updated at each AMF/VCD iteration step, and our iteration formula now reads

$$V^{(n+1)} = \frac{\frac{E}{M^{(n)}} + \Phi G^{(n)} A^{(n)}_{cloud}}{(1-\Phi)A^{(n)}_{clear} + \Phi A^{(n)}_{cloud}}. \tag{6}$$

The iterative AMF/VCD algorithm is straightforward to implement, and a flow diagram of the GDP 4.0 application is shown in Figure 4.

[31] For NO_2, the algorithm is simpler; there is no AMF/VCD iteration, and no molecular Ring correction: the DOAS slant column fitting result is used directly in the AMF conversion to the vertical column.

3.2. Ozone Profile-Column Map

[32] The first column-classified ozone profile data set was developed for the TOMS Version 7 (TV7) algorithm [*Wellemeyer et al.*, 1997]. The TV7 climatology has only three broad hemispherical latitude zones and no temporal classification, and it was found to be unrepresentative in some situations (an example is the use of fixed amounts of ozone in the lowest two partial columns in the tropics). A new climatology has recently been released for TOMS version 8 (P. K. Bhartia, Algorithm theoretical baseline document, TOMS v8 total ozone algorithm, available at http://toms.gsfc.nasa.gov/version8/version8_update.html) and this was used for GDP 4.0. This has a more sophisticated classification scheme than its predecessor, with 12 monthly profiles in 18 latitude zones at 10° intervals. The TV8 data has a variable column classification, from 3 to 5 columns at tropical latitudes and as much as 11 columns for polar regions. Column amounts vary from 125 DU to 575 DU

and are separated at 50 DU intervals. Profile partial column amounts are also given in Dobson units.

[33] The total ozone column V is the sum of the partial columns $\{U_j\}$ that make up a given ozone profile, where j is an index for the atmospheric layering. In the TV8 climatology, we are given a number of partial column profiles corresponding to fixed total column amounts. The profile-column mapping establishes the profile to be used for arbitrary values of the total column. For the linear profile-column map, the desired profile is expressed as a linear combination of two adjacent profiles $\{U_j^{(1)}\}$ and $\{U_j^{(2)}\}$ with corresponding total columns $V^{(1)}$ and $V^{(2)}$ bracketing V:

$$U_j(V) = \left(\frac{V - V^{(1)}}{V^{(2)} - V^{(1)}}\right) U_j^{(2)} + \left(\frac{V^{(2)} - V}{V^{(2)} - V^{(1)}}\right) U_j^{(1)}. \quad (7)$$

If the vertical column lies outside the range of values classifying the climatology, we extrapolate with splines: this situation may occur in extreme ozone hole scenarios ($V <$ 125 DU). Latitude and time of GOME measurements are specified from level 1 geolocation information. In order to avoid jump artifacts' associated with discrete latitude and time classifications, the climatological profiles are interpolated between latitude bands using a linear weighting scheme based on the cosine of the latitude, and over time using a linear weighting based on the day of the month.

[34] In GDP 4.0, we use the pressure grid of the ozone profile climatology for calculating layer optical properties required for the LIDORT computations. The TV8 climatology uses 11 partial columns with layer pressure differences based on atmospheric scale heights (pressures are halved for each successive atmospheric boundary). For each GOME pixel, it is necessary to adjust the lowest-layer partial column to account for the actual surface pressure (this depends for the most part on the assigned topographical height). This adjustment is done by scaling the partial column with the logarithm of the layer pressure difference. For the computation of AMFs to cloud top, the lowest layer is bounded by the cloud top pressure, and the corresponding partial column will also scale with the logarithmic pressure drop. The ghost column is the difference between clear and cloudy sky total columns, and it emerges directly from the profile-column mapping.

3.3. Radiative Transfer Model for the AMF Calculation

[35] Previous versions of GDP have used look-up tables (LUTs) for AMF determination. In GDP 3.0, LUTs were used to train a neural network ensemble for fast AMF computation. AMF LUTs are used in both the TOGOMI/TOSOMI [*Eskes et al.*, 2005] and WFDOAS [*Coldewey-Egbers et al.*, 2005] algorithms. These LUTs are large data sets with multiple classifications. In GDP 4.0, we have adopted a different approach, in which all AMFs are computed directly using a fast radiative transfer model that is able to deliver all necessary AMF results well within the data turnover rate.

[36] In GDP 4.0 we use the LIDORT radiative transfer model [*Spurr et al.*, 2001; *Spurr*, 2002] to simulate backscatter radiances I_g and I_{nog} in the AMF definition in equation (2). LIDORT is a multiple scatter multilayer discrete ordinate radiative transfer code. The atmosphere is assumed stratified into a number of optically uniform layers (in the ozone AMF computations, the layering scheme follows the TV8 pressure grid). The LIDORT code uses the pseudospherical (P-S) approximation: all scattering takes place in a plane-parallel medium, but attenuation of the solar beam before scatter is determined by ray tracing through a spherical shell atmosphere. The LIDORT code used here neglects light polarization. Although polarization in RT simulations is an important consideration for ozone profile algorithms [see, e.g., *van Oss et al.*, 2002], in DOAS retrievals with narrow fitting windows in the UV, the polarization signature is subsumed in the closure polynomial.

[37] The P-S approximation is sufficiently accurate for AMF computations with solar zenith angle (SZA) up to 90° and for line-of-sight viewing angles up to 30°–35° from the nadir [see, e.g., *Sarkissian et al.*, 1995]. However, the P-S implementation is not accurate enough for the polar view mode of GOME (scan angles in the range 40°–50°). This requires additional corrections for beam attenuation along curved line-of-sight paths, and for this we use the LIDORT version 2.2+ [*Spurr*, 2003] which possesses this line-of-sight correction. LIDORT V2.2+ is used for all viewing modes in order to maintain consistency.

[38] Another issue concerns the change in scan angle across a GOME pixel. Simulated radiances should be integrated over the readout time. This is especially important for the GOME back scan in order to account for the greater scan angle range (±31°) and the longer readout (6 s as opposed to 1.5 s for the nominal forward scans). In GDP 3.0 for both forward and backward scans, the three level 1 geolocation geometries (specified at the start, midpoint and end of scan) were used as inputs to three separate radiance simulations, which were then combined in the ratios 1:4:1 (parabolic integration of spot radiance over scan angle). The issue of scan angle integration of radiance has been looked at more systematically for GOME ozone profile retrievals (R. van Oss, private communication, 2001). When considering the integration of radiances over the readout duration, one should take into account that the scan mirror does not move uniformly with time for part of the back scan. It was found that an approximation of the scan angle integration by means of two-point Gauss-Legendre quadrature gives good accuracy for most radiance simulations. This scheme was adopted for GDP 4.0 forward scans. Further simulations have shown that a three-point quadrature gives sufficient accuracy for back scans, and this scheme was adopted for back scans.

[39] For DOAS applications with optically thin absorbers, the trace gas AMF wavelength dependence is weak and it is customary to choose the midpoint wavelength of the fitting window. This does not apply to ozone in the 325–335 nm DOAS fitting window, and for GDP versions up to and including 3.0, the O_3 AMF was always calculated at 325.0 nm. The motivation and explanation for this choice of wavelength are given by *Burrows et al.* [1999a]. Further testing of the AMF wavelength choice was done using simulated level 1 GOME radiances of *Van Roozendael et al.* [2002], and it was shown that with this choice of 325.0 nm, total ozone errors of up to 5% are possible for solar zenith angles in excess of 80°, and generally, errors at the 0.5–1% level are found for Sun angles <80°. In the

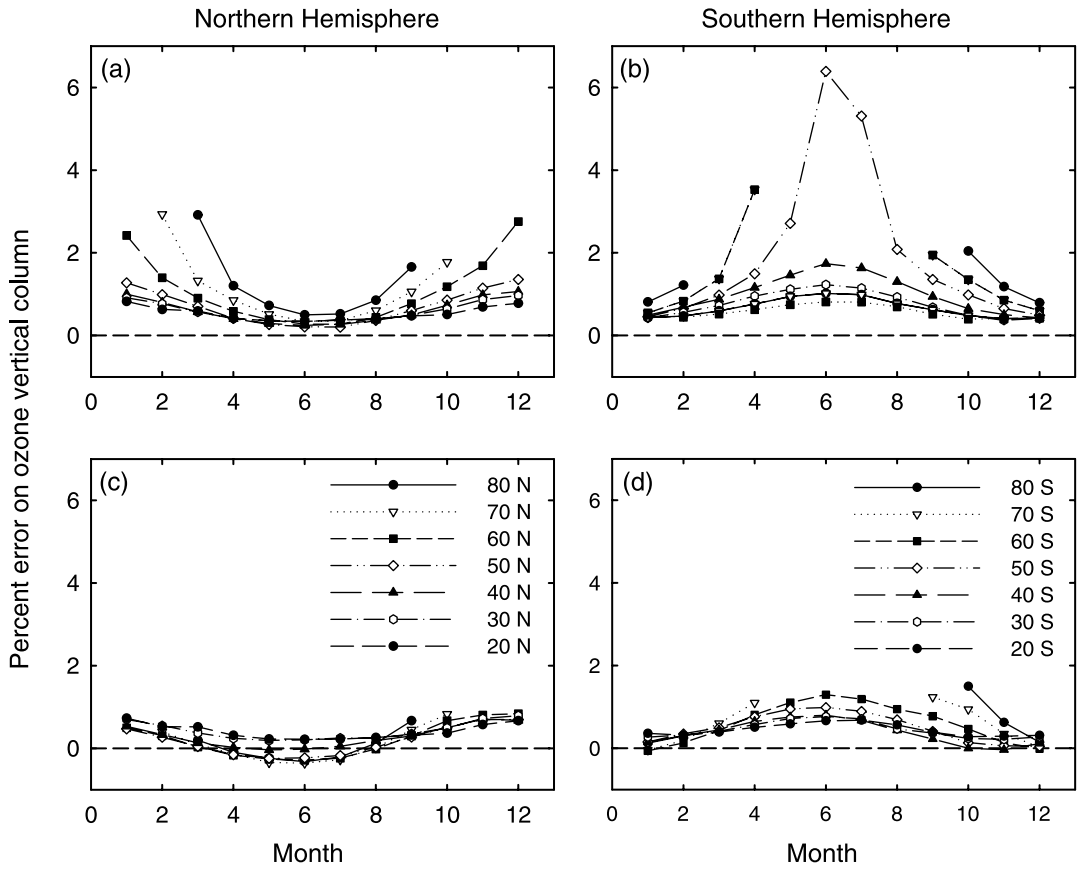

Figure 5. Impact on the total ozone accuracy of the choice of single wavelength for ozone AMF computations. Retrievals were made using synthetic radiance data based on the ozone profile climatology of *Fortuin and Kelder* [1998] (12 months, seven latitude bands, both hemispheres). (a and b) Percentage error on total ozone columns for AMFs calculated at 325.0 nm. (c and d) Percentage error on total ozone with AMFs at 325.5 nm.

same study, it was shown that these errors are reduced (to the 1–2% level for SZA > 80°) when 325.5 nm is used as the representative AMF wavelength. The impact of the change in wavelength for the computation of the ozone AMFs is illustrated in Figure 5. The ozone vertical column error displayed in Figures 5c and 5d includes all basic aspects of the DOAS retrieval approach adopted for GDP 4.0 (except for cloud effects), and can be regarded as the "best-case "accuracy that can be expected from actual GOME retrievals. Errors below 1% are obtained in all typical GOME observation conditions, which is compliant with requirements on GOME total ozone accuracy, given the size of error sources in actual measuring conditions.

[40] LIDORT is pure scattering code, and requires as input the following optical properties in each layer: (1) total extinction optical thickness, (2) total single scatter albedo, and (3) total phase function scattering coefficients. LIDORT also requires knowledge of the surface reflection (assumed Lambertian). In the GDP 4.0 application, there is an "atmospheric/surface setup module" which deals with detailed radiative transfer physics of molecules, trace gases, aerosols, clouds and surface reflection as needed to create the necessary LIDORT inputs. This setup function is completely decoupled from LIDORT, and this gives the AMF computation great flexibility. It is straightforward to change input climatology and other reference atmospheric and surface data sets. The setup function is described in the next section.

3.4. Atmospheric and Surface Setups for the RT Model

[41] As noted above, GDP 4.0 uses pressure levels from the TV8 ozone profile climatology. Top of the atmosphere (TOA) is set at 0.03 hPa. Temperature profiles are required for hydrostatic balance and the determination of ozone cross sections. GDP 4.0 uses a zonal mean (18 latitude bands) and monthly mean temperature climatology that is supplied with the TV8 ozone profiles. Altitudes are determined by hydrostatic balance, with the acceleration due to gravity varying with latitude and height according to the specification by *Bodhaine et al.* [1999]. For surface topography, GDP 4.0 uses the GTOP30 topographical database (http://lpdaac.usgs.gov/gtopo30/gtopo30.asp). In the calculation of ozone absorption optical thickness, the preshifted GOME flight model O_3 cross sections (as used in the DOAS fitting) are interpolated quadratically to account for the temperature dependence.

[42] Rayleigh scattering is determined from a standard formula, but using the latest parameterizations as given by *Bodhaine et al.* [1999]. The Rayleigh phase function depolarization ratio is taken from [*Chance and Spurr*, 1997]. In

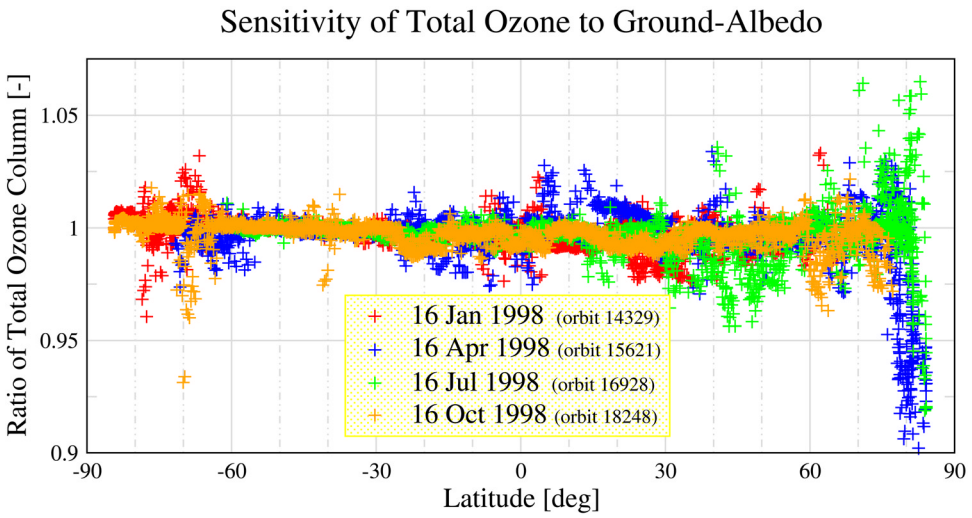

Figure 6. Ratios of total ozone columns retrieved with the GDP 4.0 algorithm. Columns are calculated first using the new GOME/TOMS LER data set and then divided by corresponding column amounts based on the static surface albedo climatology as used in the GDP 3.0 [*Matthews*, 1983; *Bowker et al.*, 1985]. The ratios have been plotted for four orbits in the different seasons of 1998.

GDP 4.0 total ozone retrievals, aerosols are neglected in the AMF computations, since AMF and VCD values are insensitive to aerosols to first order. For sensitivity testing, we have used the MODTRAN aerosol data sets [*Kneizys et al.*, 1988; *Berk et al.*, 1989] to provide aerosol loading and optical properties. We return to the aerosol sensitivity issue in section 6.2 below.

[43] The static surface albedo climatology used in GDP 3.0 [*Matthews*, 1983; *Bowker et al.*, 1985] has been replaced in GDP 4.0 with a dynamic albedo data set derived from accumulated satellite reflectance data. We use a combination of the GOME Lambertian equivalent reflectivity (LER) data set of albedos prepared from 5.5 years of reflectivity data [*Koelemeijer et al.*, 2003], and the Nimbus 7 TOMS LER data set prepared from 14.5 years of data from 1978 [*Herman and Celarier*, 1997], and valid for 340 and 380 nm. The GOME LER data has monthly and yearly entries on a $1^\circ \times 1^\circ$ latitude/longitude grid, at 12 different wavelengths spanning the GOME range; the TOMS data is also monthly. We use GOME LER data at 335 and 380 nm, and TOMS LER data at 380 nm; the desired combination albedo is $a(\lambda) = s(\lambda)a_{\mathrm{TOMS}}(380)$, where the scaling is $s(\lambda) = a_{\mathrm{GOME}}(\lambda)/a_{\mathrm{GOME}}(380)$, and λ = 335 nm for total ozone fitting [*Boersma et al.*, 2004]. In this way, the strengths of both data sets are combined: the long duration of the TOMS record (1978–1992) and the spectral information (11 wavelengths) of the shorter GOME record (1995–2001).

[44] Changes in surface albedo values will chiefly affect the clear-sky AMF A_{clear} and the intensity-weighted cloud fraction Φ. The effect on the total ozone column is largest for cloud-free and partly cloudy scenes; for completely cloud-covered scenes the effect is generally small, since the clear-sky AMF plays no part in the total ozone column calculations (see equation (3) with $\Phi = 1$). In Figure 6 we show the effect of this albedo database change on the total ozone columns for four GOME orbits. Note the effects of sea ice at high northern latitudes in spring (blue). Sea ice is present in the GOME/TOMS LER data set, but it was not correctly represented in the static surface albedo climatology used in GDP 3.0.

[45] In the independent pixel approximation, cloud information is reduced to the specification of 3 parameters (cloud fraction, cloud top albedo and cloud top pressure). Clouds are regarded as highly reflecting Lambertian surfaces. GDP 4.0 employs the OCRA and ROCINN cloud preprocessing steps before the total column retrieval. OCRA uses the GOME subpixel PMD output and it delivers the geometric cloud fraction [*Loyola and Ruppert*, 1998; *Loyola*, 2000]. ROCINN [*Loyola*, 2004] is a new fitting algorithm using O_2 A band reflectivities from GOME, and it retrieves cloud top pressure and cloud top albedo. Cloud fraction in the ROCINN algorithm is constrained to take the OCRA value when the algorithms are used in tandem. The algorithms are summarized in section 5. The GDP 4.0 algorithm can ingest cloud results derived offline from other algorithms. In particular, values of effective cloud fraction and cloud top pressure from the FRESCO O_2 A band algorithm [*Koelemeijer et al.*, 2001] were used in the verification phase and for validation purposes.

4. Molecular Ring Correction

4.1. Introduction

[46] The smoothing (“filling-in”) of Fraunhofer features in zenith sky spectra was reported by *Grainger and Ring* [1962] and has become known as the Ring effect. It is also present in satellite instruments measuring in the UV and visible. It is now known to be caused in large part by inelastic rotational Raman scattering (RRS) from air molecules. The Ring reference spectrum is defined as the change in optical depth between intensities calculated with and without RRS. The Ring effect is generally small, as RRS contributes only 4% of all scattering by air molecules. The Ring effect shows up best in spectral regions of significant intensity modulation such as the well known Fraunhofer Ca II lines around 394–398 nm. However, modulations of

backscattered light in the ozone Huggins bands are also large enough for inelastic RRS effects to appear as the filling-in of ozone absorption features (the molecular or telluric Ring effect). Spectral dependence in this molecular Ring effect correlates quite strongly with the behavior of the ozone absorption.

[47] As noted in section 2.1, the Ring effect is treated as "pseudoabsorber" interference in the DOAS algorithm using a Ring reference spectrum and additive fitting parameter. It was found that neglect of the telluric Ring effect in GDP 3.0 leads to systematic underestimation of ozone total columns (up to 10%) [*Van Roozendael et al.*, 2002]. From this study, a correction for the molecular Ring effect in ozone retrieval was developed during the GOME geophysical validation campaign in 2002. A full description of this correction will be provided in a forthcoming paper and here we give a summary of the principal equations and discuss the GDP 4.0 implementation.

[48] Considering only O_3 absorption, the correction is based on a simplified forward model of the intensity at satellite $I(\lambda)$ which includes an explicit contribution due to inelastic RRS:

$$I(\lambda) = I^0(\lambda) \cdot \exp\left[-\sigma_{O3}(\lambda) \cdot E_{O3} - P_1^{\lambda}\right] + E_{Ring} \cdot I_0^{RRS}(\lambda) \cdot \exp\left[-\sigma_{O3}(\lambda) \cdot E_{O3}^{RRS} - P_2^{\lambda}\right]. \quad (8)$$

The first term on the right-hand side follows the Lambert-Beer law for ozone absorption, with $I^0(\lambda)$ the solar intensity, and σ_{O3} and E_{O3} the ozone absorption cross section and effective slant column respectively. Elastic scattering effects are subsumed by means of the low band pass polynomial P_1^{λ}. The Ring effect is modeled by the second term in equation (8), in which there are several approximations. First, it is assumed that Raman-scattered light is generated close to the surface of the atmosphere, with the spectral shape given by a source spectrum for Raman scattering $I_0^{RRS}(\lambda)$. This source spectrum only treats the spectral smoothing effect of RRS on the solar intensity. In practice it is calculated by the convolution of a GOME irradiance spectrum using Raman cross sections appropriate to inelastic scattering into the wavelength of interest. The fractional intensity of Raman light (the E_{Ring} parameter) is freely adjustable. This may vary considerably and will depend on parameters such as cloud coverage, cloud altitude and surface albedo. Ozone absorption (the term $\sigma_{O3}(\lambda).E_{O3}^{RRS}$) is then treated consistently, assuming that Raman photons produced at the surface and/or above clouds travel upward to the satellite. Ozone absorption taking place in the incoming light is assumed to be fully smeared out in the inelastic process, so that it can be neglected in the first approximation.

[49] Raman scattered light smoothes out structured information in incident solar radiation. It can be seen as a source of atmospheric stray light which produces a lowside bias on any retrieved trace gas total column. This bias will nevertheless be modulated by atmospheric absorption in light paths above the region of RRS generation in the lower troposphere. For ozone, the bulk of the column is located in the stratosphere and upper troposphere, mostly above the source of RRS. Hence ozone absorption that takes place in RRS light can be easily estimated. This is not necessarily the case for other trace gases, which may have significant partial columns in the lower troposphere. In summary, Raman scattering has a similar impact on all atmospheric absorbers, but it can only be accounted for accurately in a simple way for stratospheric trace gases such as O_3.

4.2. DOAS Implementation

[50] Equation (8) can be rewritten (after a Taylor expansion, discarding higher-order terms) in the following way:

$$\ln\left[\frac{I(\lambda)}{I^0(\lambda)}\right] = -\sigma_{O3}(\lambda).E'_{O3} - \sigma_{Ring}(\lambda).E_{Ring} - P(\lambda), \quad (9)$$

with the Ring cross section $\sigma_{Ring}(\lambda)$ defined as:

$$\sigma_{Ring}(\lambda) = -\frac{I_0^{RRS}(\lambda)}{I^0(\lambda)}. \quad (10)$$

Equation (9) is the familiar DOAS fitting model, from which E'_{O3}, E_{Ring} and the $P(\lambda)$ polynomial coefficients can be derived in the usual manner. The major difference with Ring correction methods used in previous studies comes in the definition of the modified O_3 effective slant column E'_{O3}, which is related to the effective slant column for elastic scattering (E_{O3}) by the following formula:

$$E'_{O3} \cong E_{O3}.\left\{1 + E_{Ring} \cdot \bar{\sigma}_{Ring} \cdot \left(1 - \frac{\sec(\theta_0)}{A_{total}}\right)\right\} = E_{O3}.M_{Ring}, \quad (11)$$

where A_{total} is the ozone AMF, θ_0 the solar zenith angle, and $\bar{\sigma}_{Ring}$ an average Ring cross section calculated over the spectral fitting interval. Equation (11) defines the molecular Ring correction M_{Ring}. From section 3.1, we have $A_{total} = (1 - \Phi)A_{clear} + \Phi A_{cloud}$ in the independent pixel approximation, where Φ is the intensity-weighted fractional cloud cover.

[51] In this formulation, the DOAS fitting is essentially unchanged, and it gives fitted parameters E'_{O3} and E_{Ring}. The effective slant column for ozone is then adjusted after the fit through the relation $E_{O3} = M_{Ring}\, E'_{O3}$. Note that the molecular Ring term M_{Ring} can also be used to quantify the error due to an incorrect estimation of the Ring effect in previous GDP versions. Studies have shown that for moderate SZA, the geometrical AMF is sufficiently accurate to approximate A_{total} in equation (11). For high SZA with a long path through absorbing ozone layers, a more precise calculation is needed. However, in GDP 4.0, we use the LIDORT-calculated total AMF already computed at each AMF/VCD iteration step to obtain M_{Ring} and the corrected slant column $E'_{O3} = E_{O3}/M_{Ring}$ as required for the VCD update (equation (6)).

[52] Figure 7 shows values of the molecular Ring correction term M_{Ring} for four seasonally representative GOME orbits. In GDP 3.0, ozone slant columns are clearly scaled up by 2 to 9% and this is more than enough to compensate for the negative bias observed in several GOME validation campaigns. The general shape of the correction factor is due to the variation of SZA across the GOME orbit. Pronounced peaks and high-frequency oscillations are mainly due to clouds, but changes of surface albedo and surface height can

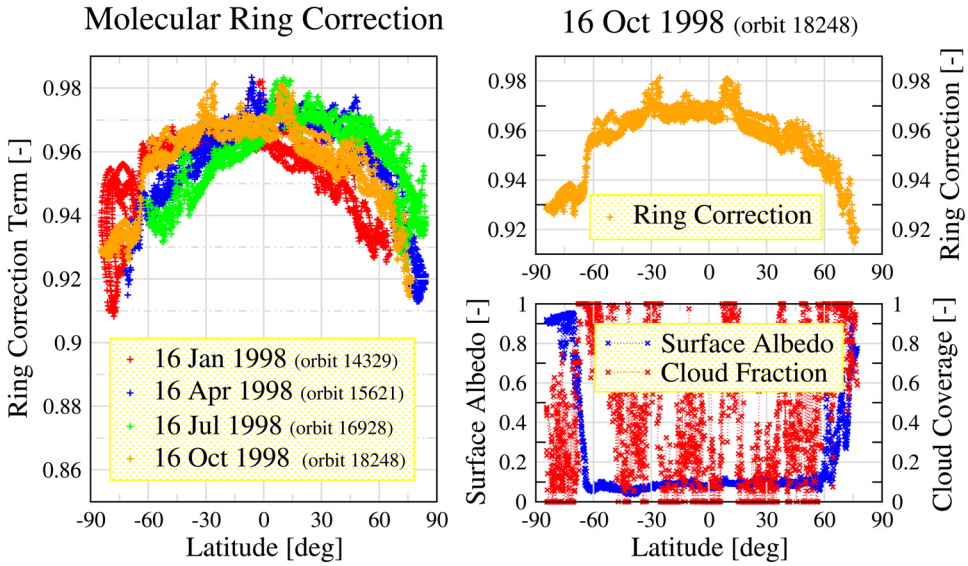

Figure 7. (left) Molecular Ring correction factors for four GOME orbits in 1998 and (right) Ring correction, surface albedo, and fractional cloud cover for one GOME Orbit. See text for more information.

influence the correction. The cloud impact is especially visible for orbit 18248 (orange) at latitudes of 10°N and 30°S where the GOME measurements were affected by high clouds and the high cloud fractional cover typically found in tropical regions. With RRS dominant in the lower troposphere, high cloud cover implies an immediately noticeable reduction in the RRS contribution to the measured radiance, and a consequent reduction in the Ring correction factor (closer to unity). The influence of the surface albedo is obvious at high southern latitudes where a sharp increase of the albedo around 60°S due to sea ice and the Antarctic ice shield is associated with a corresponding decrease of the Ring correction term.

[53] The other new algorithms for GOME total ozone both have new implementations of the Ring effect, and it is instructive to compare methodology. The technique described here is based on ideas proposed by *Van Roozendael et al.* [2002]. These ideas were further developed independently as part of the TOGOMI project and also as part of present GDP 4.0 work. As a result, the molecular Ring correction methodology in the TOGOMI/TOSOMI algorithm [*Eskes et al.*, 2005] and in GDP 4 (sections 4.1 and 4.2) are essentially identical in concept and both use the same basic assumptions. There are some differences in implementation. In TOGOMI, the DOAS fitting is nonlinear as it is based on measured reflectivities (ratios of earthshine radiance to Sun irradiance), while in GDP 4.0 we use a traditional DOAS linear fit to the log ratio of the same quantities. The definition of M_{Ring} in equation (11) appears in the TOGOMI paper, except that a geometrical AMF appears in place of A_{total}. The TOGOMI algorithm uses precomputed AMF look-up tables and there is no AMF/VCD iterative adjustment, and hence there is only one molecular Ring correction. In contrast, the WFDOAS algorithm [*Coldewey-Egbers et al.*, 2005] relies on precalculated look-up tables of Ring correction factors determined using a radiative transfer code including RRS (the SCIATRAN model [*Vountas et al.*, 1998]) and sorted as function of several parameters (solar zenith angle, total ozone, surface albedo, and surface altitude). This is a more sophisticated approach applicable in principle to all trace gas absorbers, but it requires the use of precalculated tables.

[54] The accuracy of our simplified approach has been tested under various conditions using the same SCIATRAN model as a reference. We describe here some verification tests performed using simulations of the earthshine radiances provided by the SCIATRAN code. The atmosphere was set up using ozone profiles from a seasonally classified and latitude resolved climatology [*Fortuin and Kelder*, 1998]. Simulations of synthetic radiances in the range 320–340 nm were performed at SZAs representative of GOME observations at latitudes and seasons sampled by the climatology. DOAS retrievals were then performed using configuration settings as they appear in operational GOME retrievals. In Figure 8, errors on the retrieved ozone slant columns are compared for retrievals performed with a basic "Fraunhofer-only" Ring correction (as in GDP 3.0), and retrievals using the new correction method developed for GDP 4.0. The underestimation in the absence of molecular Ring correction lies in the range 5–10% and shows clear solar zenith angle dependence. This systematic underestimation is largely compensated by the new correction, for all conditions applied in the tests. Comparable results were obtained for the WFDOAS algorithm [*Coldewey-Egbers et al.*, 2005], as well as for the TOGOMI algorithm [*Eskes et al.*, 2005].

5. Cloud Preprocessing

[55] Earlier versions of GDP used the ICFA algorithm [*Kuze and Chance*, 1994] to retrieve cloud fraction from O_2 A band reflectances, with other cloud properties derived from climatology. By contrast, GDP 4.0 uses two new algorithms for generating cloud information inputs for the main ozone retrieval. These two cloud preprocessing algo-

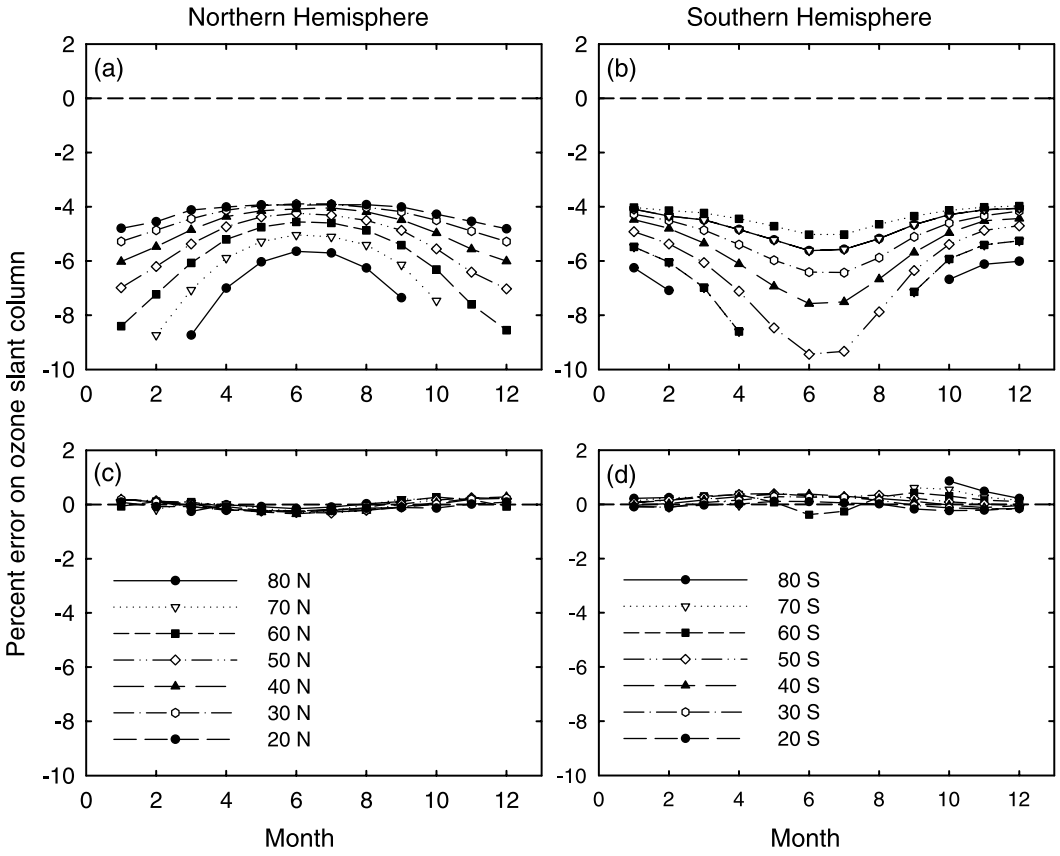

Figure 8. Ring effect tests using synthetic data calculated with the SCIATRAN model based on the ozone profile climatology of *Fortuin and Kelder* [1998] (12 months, seven latitude bands, both hemispheres). (a and b) Percent error on retrieved ozone slant column when not accounting for molecular filling-in (GDP 3.0 baseline); (c and d) Percent error on retrieved slant column after application of the new Ring effect treatment (GDP 4.0 baseline).

rithm are summarized in the next two sections, along with a short digest of their validation (section 5.3).

5.1. OCRA

[56] The basic idea in optical cloud recognition algorithm (OCRA) [*Loyola and Ruppert*, 1998] is to break down each optical sensor measurement into two components: a cloud-free background and a residual contribution expressing the influence of clouds. The key to the algorithm is the construction of a cloud-free composite that is invariant with respect to the atmosphere, to topography and to solar and viewing angles. For a given location (x,y), we define a reflectance factor $\rho(x,y,\lambda)$ measured by the PMDs of GOME at wavelength λ for the ground cover projection of the image. This reflectance is translated into normalized *rg* color space via the relation:

$$r = \frac{\rho(x,y,\lambda_R)}{\sum\limits_{i=R,G,B}\rho(x,y,\lambda_i)}, g = \frac{\rho(x,y,\lambda_G)}{\sum\limits_{i=R,G,B}\rho(x,y,\lambda_i)}. \quad (12)$$

If M is the set of n normalized multitemporal measurements over the same location (x,y), then a cloud-free (or minimum cloudiness) pixel rg_{CF} in M is selected with the brightness criterion $\|rg_{CF} - w\| \geq \|rg_k - w\|$ for $k = 1,.,n$, where $w = (1/3,1/3)$ is the white point in the *rg* chromaticity diagram. A global cloud-free composite is constructed by merging cloud-free reflectances $\rho_{\mathrm{CF}}(\lambda)$ (corresponding to rg_{CF}) at all locations. The effective cloud fraction is determined by examining separations between RGB reflectances and their cloud-free composite values:

$$c_f = \sqrt{\sum_{i=R,G,B_i}\alpha(\lambda_i)\max\left(0,[\rho(\lambda_i)-\rho_{CF}(\lambda_i)]^2-\beta(\lambda_i)\right)}. \quad (13)$$

Scaling factors α ensure that the cloud fraction is mapped to [0, 1], while offsets β account for aerosol and other radiative effects. A detailed description is given by *Loyola* [2000].

5.2. ROCINN

[57] ROCINN [*Loyola*, 2004] is a new algorithm based on O_2 A band reflectances from GOME: it delivers cloud top pressure and cloud top albedo. The independent pixel approximation is used; the cloud fraction c_f derived from the OCRA algorithm is taken as a fixed input to the ROCINN algorithm. In the simulations, only attenuation through oxygen absorption of the direct solar beam and its reflection from ground or cloud top is considered. Molecular scattering, scattering and absorption by aerosols and diffuse surface reflection are neglected, as is absorption by oxygen within and below any clouds. Surfaces are assumed to be

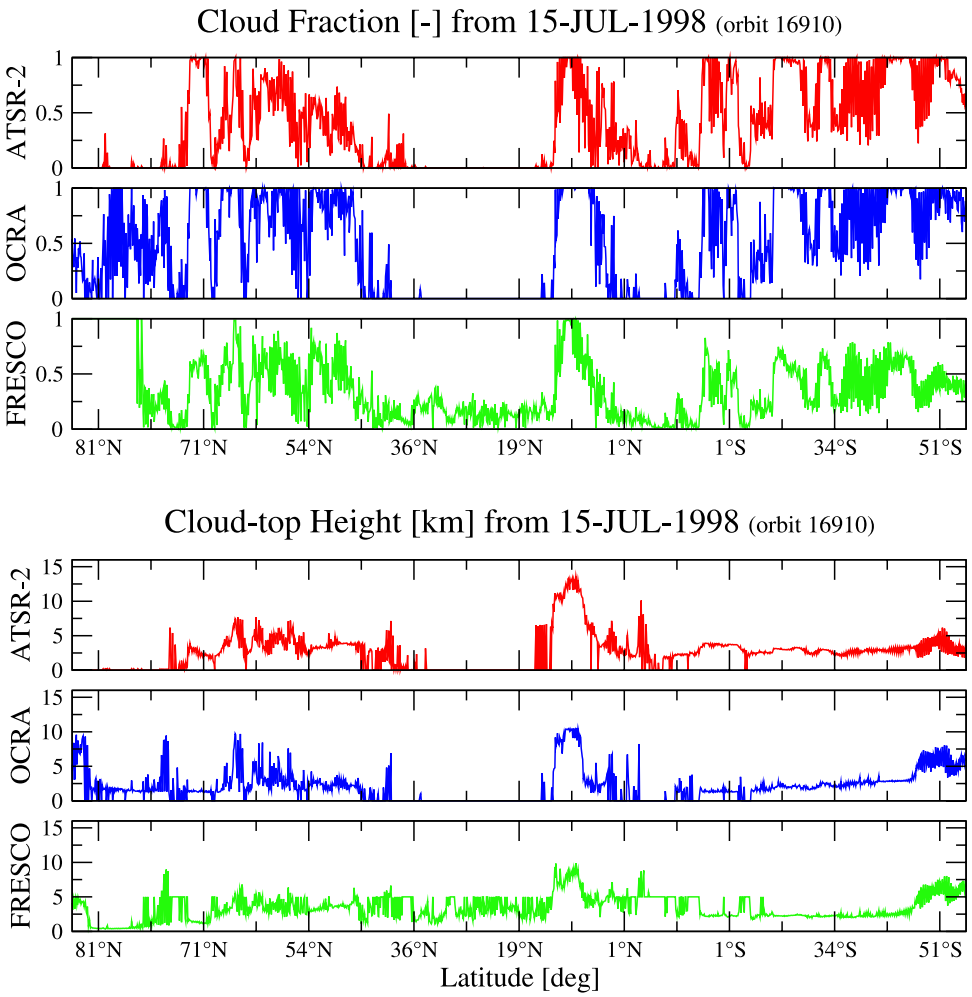

Figure 9. (top) Comparison of cloud fraction retrieved from ATSR-2 and from GOME using the OCRA and FRESCO algorithms. (bottom) Comparison of cloud top height retrieved from ATSR-2, and from GOME using ROCINN and FRESCO.

Lambertian reflectors. In this approximation, we need only consider transmittances along two photon paths through the atmosphere, and the forward model reflectivity is then:

$$R_{sim}(\lambda) = c_f \langle T_c(\lambda, \Theta, c_a, c_z)\rangle + (1 - c_f)\langle T_s(\lambda, \Theta, s_a, s_z)\rangle \quad (14)$$

Here $\langle T\rangle$ denotes the convoluted transmittance to cloud top or surface for path geometry Θ (solar zenith angle and line-of-sight angle), wavelength λ, surface albedo s_a and cloud top albedo c_a, and lower boundary heights s_z (surface) and c_z (cloud top). Line-by-line transmittances must first be calculated using line spectroscopic information for the O_2 A band (taken from the HITRAN database [*Rothman et al.*, 2003]), before convolution with the GOME slit function. Quantities s_z and s_a are the surface height and albedo, taken from a suitable database and assumed known. ROCINN aims to retrieve cloud top height c_z and the cloud top albedo c_a. Transmittance calculations based on equation (14) are used to create a complete data set of simulated reflectances for all viewing geometries and geophysical scenarios, and for various combinations of cloud fraction, cloud top height and cloud top albedo. High-resolution transmittances are computed for the range 758–772 nm at resolution 0.002 nm before convolution.

[58] In ROCINN, the forward model function is represented by the set $S = \{(X_i, Y_i)\}$ for $i = 1,\ldots,s$. Inputs X are the parameters $\{c_f, \Theta, s_a, s_z, c_a, c_z\}$. The outputs Y are the simulated radiances $\{R_{sim}(\lambda)\}$. To generate an inverse data set, we first add normal distributed Gaussian measurement noise ε to the simulated radiances: $R = R_{sim} + \varepsilon$. We may now generate the inverse data set $S^* = \{(X_i^*, Y_i^*)\}$ for $i = 1,\ldots,t$, where now the input set X^* comprises the parameters $\{R_{sim}(\lambda), c_f, \Theta, s_a, s_z\}$ and the output is now $Y^* = \{c_a, c_z\}$, the unknown cloud top albedo and cloud top height. A neural network NN_{INV} is finally trained with the *inverse* data set S^*, giving the result

$$\{c_a, c_z\} = NN_{INV}\left(R_{sim}(\lambda), c_f, \Theta, s_a, s_z\right) \quad (15)$$

For more details on the use of neural networks to solve inverse problems, see *Loyola* [2004].

[59] The ROCINN, ICFA [*Kuze and Chance*, 1994], and FRESCO [*Koelemeijer et al.*, 2001] algorithms all use the O_2 A band reflectances from GOME. However, the algorithms have differences in content and methodology. ROCINN retrieves cloud top height and cloud top albedo

taking the OCRA cloud fraction as a fixed input. ICFA retrieves only the cloud fraction and takes a predefined cloud top height from climatology and assumes a fixed cloud albedo of 0.8. FRESCO retrieves the effective cloud fraction and cloud top height, also assuming a fixed cloud albedo of 0.8. The other main difference lies with the inversion method: ROCINN computes the inverse function using neural network techniques, while ICFA and FRESCO perform the inversion using nonlinear least squares minimization between measured and simulated reflectances.

[60] GOME is not able to distinguish between cloud cover and snow/ice surface conditions, as the instrument does not possess infrared channels. Furthermore, GOME is not sensitive to optically thin cirrus clouds. Despite these caveats, it is worth remarking that the cloud fraction is retrieved under all surface conditions; for snow/ice scenarios, OCRA will return an overestimate of the cloud fraction. Similarly, the cloud top height and cloud top albedo are retrieved for all pixels flagged as partially or fully cloudy.

[61] In GOME scenes for which OCRA has overestimated (underestimated) the cloud fraction, ROCINN will compensate by underestimating (overestimating) the cloud top albedo and slightly overestimating (underestimating) the cloud top height. The influence of possible cloud parameter inaccuracies on the retrieved ozone total column is discussed on section 6.2.

5.3. OCRA/ROCINN Verification

[62] These algorithms were verified by comparison with ATSR-2 data. ATSR-2 measures simultaneously with GOME on ERS-2, but it has a smaller field of view (pixel resolution ~1.1 km), so GOME narrow swath orbits were selected. Cloud fraction and cloud top height are determined from ATSR-2 data using infrared brightness temperature algorithms and the instrument's stereo viewing capability. ATSR-2 measurement data for one year (April 1998 to March 1999) were used in the verification (331 orbits). These were obtained by means of a retrieval scheme developed at the Rutherford Appleton Laboratory for the specific purpose of characterizing clouds in the GOME field of view [*Siddans et al.*, 1999]. OCRA/ROCINN and FRESCO results were compared with this data set. Cloud top albedo was not available from ATSR-2.

[63] The cloud fraction determined with OCRA, FRESCO and ATSR-2 in 15 July 1998 is shown in Figure 9 (top). In general, OCRA results are close to those for ATSR-2, while FRESCO has a tendency to underestimate the ATSR-2 results as it computes an effective cloud fraction assuming a fixed cloud albedo. This ATSR-2 comparison confirms the results reported by *Tuinder et al.* [2004] where several algorithms for retrieving cloud fraction using GOME data were compared against synoptic surface observations: in this work, OCRA has a mean difference of −10% compared with synoptic data, compared to FRESCO (−19.7%) and ICFA (−38.9%). Cloud top heights determined with ROCINN, FRESCO and ATSR-2 for a 15 July 1998 orbit are shown in Figure 9 (bottom). In general, the three algorithms provide similar results, with ROCINN and FRESCO tending to underestimate the cloud top height. The latter effect is mainly due to the treatment of clouds as reflecting boundaries compensating for the neglect of oxygen absorption inside the clouds. ROCINN is smoother and more stable than FRESCO and has fewer spikes. ROCINN computes realistic cloud top height values even for pixels with low cloud fraction; for FRESCO, a default value of 5 km is fixed for pixels with a cloud fraction <0.1. ROCINN does not produce outliers most likely because the neural network is robust and it finds a global minimum solution to the inverse function. The cloud top height cannot be retrieved for cloud-free scenes (e.g., between 35°N to 20°N). In this case, both ATSR-2 and ROCINN report a cloud top height of zero, while FRESCO reports cloud fractions up to 0.2 and cloud top heights of 2–5 km.

[64] The suitability of a cloud retrieval algorithm for trace gas retrieval is very difficult to assess, as clouds influence most quantities appearing in equation (6), the iterative AMF/VCD method. With this in mind, the aim of the verification is to demonstrate that the GOME-retrieved cloud information is accurate and that it does not show systematic errors. ATSR-2 comparisons show that OCRA/ROCINN gives better results on average than those from FRESCO. Differences in fraction and cloud top height are smaller, and standard deviations of these differences are lower. Cloud top heights from the ROCINN algorithm also show reduced scatter against ATSR-2 values.

[65] A discussion of the influence of clouds and particularly of the effects of cloud fraction uncertainty on the total ozone error is given in section 6.2.

6. Error Budgets and Sensitivity Studies

6.1. Error Budgets for the Total Ozone Algorithm

[66] Referring to equation (3) in section 3.1, the error on vertical column V (denoted as s_V) can be expressed as a function of the error on component parameters E (ozone slant column), G (ghost vertical column), Φ (radiance-weighted cloud fraction), A_{clear} (AMF for a clear sky scene), A_{cloud} (AMF to cloud top). A complete definition can be derived from error propagation rule:

$$s_V^2 = \left(\frac{\partial V}{\partial E}\right)^2 \cdot s_E^2 + \left(\frac{\partial V}{\partial A_{clear}}\right)^2 \cdot s_{A_{clear}}^2 + \left(\frac{\partial V}{\partial A_{cloud}}\right)^2 \cdot s_{A_{cloud}}^2 + \left(\frac{\partial V}{\partial \Phi}\right)^2 \cdot s_\Phi^2 + \left(\frac{\partial V}{\partial G}\right)^2 \cdot s_G^2. \quad (16)$$

[67] This error propagation formula is strictly valid under the assumption that error sources are mutually uncorrelated. In general we would expect some correlations (for example between the cloud fraction, and cloud top height and cloud top albedo, as described in section 6.2 below), but the derivation of a complete error covariance for all sources is beyond the scope of the present work. With this in mind, we may use the definition of V in equation (3) to obtain

$$\frac{\partial V}{\partial E} = \frac{1}{A_T}; \qquad \frac{\partial V}{\partial G} = \Phi \cdot \frac{A_{cloud}}{A_T};$$
$$\frac{\partial V}{\partial \Phi} = \frac{1}{A_T}[V \cdot A_{clear} - (V - G) \cdot A_{cloud}];$$
$$\frac{\partial V}{\partial A_{clear}} = -\frac{V}{A_T}(1 - \Phi); \qquad \frac{\partial V}{\partial A_{cloud}} = -\frac{\Phi}{A_T}(V - G).$$
$$A_T = (1 - \Phi)A_{clear} + \Phi A_{cloud}$$

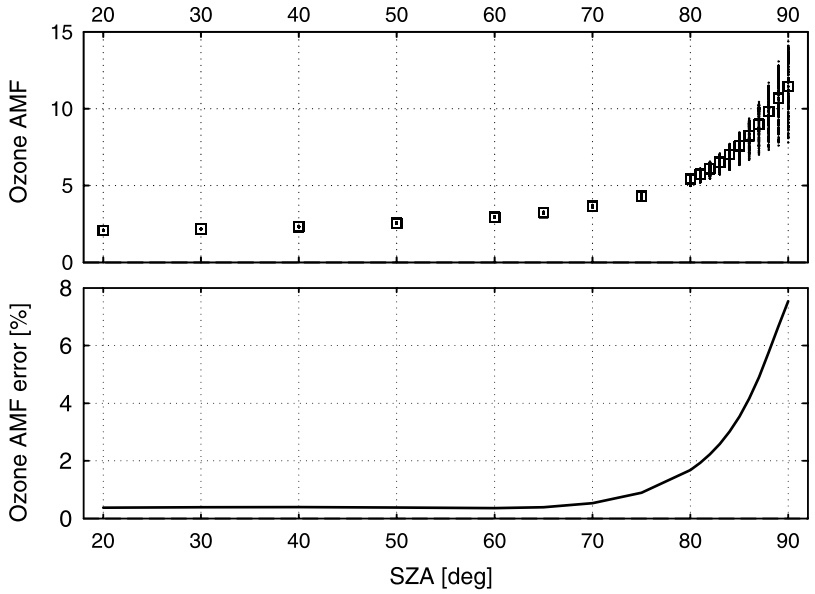

Figure 10. (top) Ozone AMF variability based on the *Fortuin and Kelder* [1998] climatology. (bottom) Ozone AMFs, percentage error as a function of SZA.

[68] Error component s_E comes from the DOAS slant column fitting, and s_Φ from the OCRA cloud preprocessing. In GDP 3.0, s_G is set to zero and a fixed value of 1% is assumed for AMF errors. In GDP 4.0, we use an AMF error that is dependent on the solar zenith angle and the ghost column error is taken as $s_G = 30\%$. As discussed below (see Figure 10), the solar zenith angle dependency of the AMF error has been determined empirically from an examination of the variability of the O_3 AMFs over a wide range of ozone profiles. It should be noted that this simplified error formulation is introduced for the calculation of the errors on a pixel-by-pixel basis, and it only includes the largest contributors to the total error budget.

[69] A more comprehensive estimation of the error budget is provided in Table 2. This includes typical errors on ozone slant columns, ozone AMFs, cloud fractions and ozone ghost columns as reported in the GDOAS delta validation report [*Van Roozendael et al.*, 2004]. The GDOAS error budget has been separated into two parts: errors affecting the retrieval of slant columns (DOAS-related errors) and errors affecting the conversion of slant columns into vertical columns (AMF-related errors). Since several AMF-related error sources are significantly enhanced at large SZA, the AMF-related part of the GDOAS error budget has been divided into two regimes (SZA < 80°, and SZA $\geq$ 80°).

[70] The DOAS-related (slant column) uncertainties quoted in Table 2 are for the most part extracted from the study associated with the GDP 3.0 Delta validation [*Van Roozendael et al.*, 2002]. Error values are determined from a number of sensitivity tests dealing with the impact of uncertainties on absorption cross sections and their temperature dependence, as well as wavelength calibration and convolution issues. We include the molecular Ring effect error under the DOAS heading. Errors due to the molecular Ring effect are derived from retrieval tests using synthetic radiance data, as presented in the GODFIT validation report [*Van Roozendael and Spurr*, 2003].

[71] Errors relating to O_3 AMF values are determined from a series of sensitivity tests carried out using different settings for the AMF calculations (e.g., different O_3 profile climatologies, or the error from the assumption of a single wavelength choice for the AMF calculation). In addition, the impacts of surface albedo errors as well as cloud and aerosol uncertainties have been considered explicitly. Several error sources are significantly enhanced at large solar zenith angles (typical of polar spring and autumn observations), and this justifies the division in the error budget in

Table 2. Estimation of Error Sources of the GDOAS Total Ozone Retrievals[a]

	Percent Error	
Error Source	SZA < 80°	SZA > 80°
Ozone slant column		
O_3 absorption cross sections	<2	<2
Atmospheric (effective) temperature determination	<1.5	<3
Instrument signal to noise	0.5	<2
Instrument spectral stability (wavelength registration)	0.5	0.5
Solar I_0 effect	0.2	0.2
Ring and molecular ring effect	<2	<2
Ozone air mass factor		
Single wavelength calculation (325.5 nm)	<1	<2
O_3 profile	<1	<4
Surface albedo	0.3	0.3
Cloud fraction	0.8	0.8
Cloud top pressure (height)	1	1
Cloud top albedo	0.8	0.8
Ghost column	<2	<3
Tropospheric aerosols	0.2	0.2
Ozone vertical column (accuracy)		
Clear	<3.6	<6.4
Cloudy	<4.3	<7.2
Ozone vertical column (precision)		
Clear	<2.4	<4.9
Cloudy	<3.3	<5.9

[a]As reported in the GDOAS validation report [*Van Roozendael et al.*, 2004].

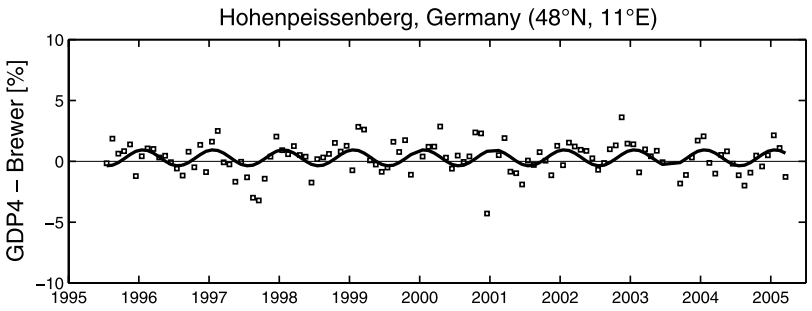

Figure 11. GDP 4–Hohenpeissenberg Brewer monthly mean ozone differences from July 1995 until April 2005. A sinusoidal fit to the time series (thick solid line) highlights the size of seasonal variations in the differences (amplitude: 0.5%). The mean bias over the 10-year time period is 0.3%.

Table 2 between values representative of solar zenith angles lower than and greater than 80°. Independently of albedo and cloud/aerosol effects, errors on AMFs will depend significantly on the shape of the ozone profile as well as its column content. Hence an upper limit of the AMF error (and its SZA dependence) can be obtained from consideration of the variability of O_3 AMFs calculated using a wide range of climatological ozone profiles. This has been done in Figure 10 (top) for calculations based on the *Fortuin and Kelder* [1998] climatology. It is evident that the AMF variability is a strong function of the SZA, especially above 80°.

[72] In an attempt to parameterize the main dependency of the AMF error, we have assumed that the AMF uncertainty can be linked to atmospheric profile shape errors, which will have a larger impact at high SZA values as indicated by the variability curve in Figure 10 (top). For operational implementation in GDP 4.0, this curve has been used to derive an empirical relationship between AMF uncertainty and solar zenith angle. A simple scaling (by a factor of 2) has been applied to the variability curve in such a way that the resulting error curve shown in Figure 10 (bottom) matches up with the error estimates shown in Table 2 for both SZA ranges. Although it is not the result of a rigorous error analysis, this empirical parameterization has the advantage of providing realistic uncertainties on the GDP 4.0 total ozone product both at low and at high SZA.

[73] The ghost column estimate of 30% used in GDP is a composite value based on error contributions from a number of sources (in particular, the ROCINN estimate of cloud top height error and the uncertainty on the tropospheric part of the ozone profile).

6.2. Sensitivity Issues for GDP 4.0 Algorithm

[74] In GDP 4.0, the largest impact of atmospheric temperature is through the temperature dependence of the ozone absorption cross sections. Two ozone spectra at two different temperatures are used in the DOAS fitting; the accuracy of this approach (see *Lambert et al.* [2002] for validation results) is limited (1) at large SZA, due to the breakdown of the optically thin approximation, (2) at extreme stratospheric temperatures (due to nonlinearity in the temperature dependence of the ozone cross sections), and (3) by the intrinsic accuracy of the laboratory cross sections. It is possible that instrument degradation also has an impact on the accuracy of the effective temperature determination. This has not been tested explicitly, but results from overpass processing over Hohenpeissenberg and Lauder, extending from 1996 until 2003 and retrieved with no particular attempt to compensate for known GOME degradation problems, suggest that the DOAS algorithm is stable and not strongly influenced by the degradation of the instrument (see Figure 11 and also *Van Roozendael et al.* [2004, Figures 4 and 5]).

[75] As noted already, the long-term stability of the GOME total ozone record is a key consideration for trend analysis. In Figure 11, monthly mean ozone differences between GDP 4.0 and Brewer measurements at Hohenpeissenberg are shown for a 10-year period from July 1995 through April 2005. A sine function has been fitted to the time series in order to highlight seasonal variations in the differences. The amplitude of these variations is about 0.5% and the mean bias is 0.3%. The long-term stability of GOME and the absence of any significant time-dependent bias are clear. It is worth noting that the stability is still evident after more than 8 years, despite some loss of ozone accuracy from June 2003 to December 2004 caused by the absence of daily solar calibration measurements in the GOME level 1 product during that period. This problem has been solved in the updated GOME level 1 processor; daily solar measurements are available once again for GOME data starting in January 2005. The level 1 and level 2 data from June 2003 to December 2004 will be reprocessed in the near future to provide a consistent GOME data record.

[76] Since the iterative AMF/VCD algorithm relies on an ensemble of ozone profiles to define the profile-column map needed for the iteration, the choice of ozone profile climatology is important. Ozone profile shape is a key factor controlling the accuracy of the total ozone retrieval, especially at high latitudes where the ozone profile shape sensitivity of the AMFs is enhanced by the extreme variations in the ozone field (e.g., ozone hole) combined with large solar zenith angles. The GDP 4.0 code has been tested using both the TOMS Version 7 and Version 8 ozone profile climatologies. Differences in retrieved total ozone columns using the two climatologies are shown in Figure 12 for a sample data set consisting of 465 orbits from 1997. Largest differences are found in polar regions (especially in the southern hemisphere) close to the terminator where GOME SZAs are at their maximum. *Spurr et al.* [2005] noted that the fixed ozone burden in the troposphere was a significant

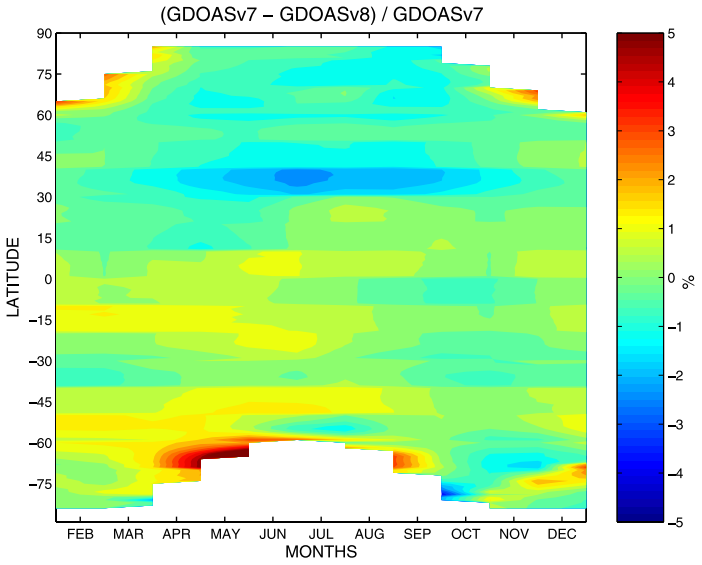

Figure 12. Relative differences in GDP 4.0 GOME total ozone retrieved using the two TOMS version 7 and version 8 ozone profile climatologies. Differences are mostly significant in polar regions, close to the terminator, and in northern tropical regions around the place of minimum GOME solar zenith angle.

error source for ozone AMFs in GDP 3.0, particularly at low SZA (maximum photon penetration). In the TV7 data set, ozone partial columns are fixed at 9 DU and 15 DU in the lowest two layers. There is much more tropospheric variation in ozone content with the Version 8 profile data, but it remains the case that errors of 10–15 DU in the tropospheric boundary layer ozone burden can induce AMF errors of 3–5% for low SZA values (~25°). This may explain the surprisingly large sensitivity in Figure 12 for the northern subtropics during summer when the GOME SZA is at minimum.

[77] It is difficult to extract any information about aerosols from a DOAS fitting of ozone in the UV Huggins bands. Aerosol scattering and extinction are subsumed in the DOAS slant column fit through the closure polynomial, and the introduction of parameterized aerosol information in the AMF RT simulations is an additional source of error. For a 10-year operational reprocessing of the GOME record, it is impossible to account for aerosol variability in anything but the simplest terms, and the policy in GDP 4.0 has been to avoid the use of aerosols altogether, and to use a Rayleigh atmosphere for the baseline AMF calculations. This contrasts with the approach used in previous GDP versions; in GDP 3.0, default aerosols from the LOWTRAN database were used on a regular basis, with the boundary layer assumed to possess a maritime aerosol regime (oceans) or a rural continental regime (land surfaces).

[78] For scattering aerosols in the troposphere, the AMF is relatively insensitive to aerosol content (generally less than 1% error). It is well known however that for scenarios with absorbing aerosols present (in particular biomass burning, industrial pollution, desert dust outbreaks and volcanic plumes), ozone AMFs may be significantly in error if the aerosol presence is ignored or not treated accordingly. These effects are again largest for low SZA.

[79] Aerosols are not treated explicitly in the GDP 4.0 AMF calculations. However, a significantly scattering aerosol layer will be detected by OCRA/ROCINN as a thin cloud layer, and the aerosol affect will thus be included indirectly in the vertical column calculation. To first order, aerosol uncertainties in the GDP 4.0 total algorithm will be picked up in the cloud parameter error budget estimates. Although cloud fractions are in general weakly influenced by the presence of aerosols, cloud algorithms such as FRESCO and OCRA/ROCINN are sensitive to strong aerosol pollution episodes.

[80] Clouds have a significant influence on the retrieved ozone total column, as most terms in equation (6) depend on cloud parameters. Both the intensity-weighted cloud fraction Φ and the Ring correction factor M depend on the three cloud parameters (cloud fraction, cloud top height and cloud top albedo). The AMF for cloudy conditions A_{cloud} depends on cloud top albedo and cloud top height, and the ghost column G depends on cloud top height. In Figure 13, we look at the effect of errors in cloud fraction from OCRA on the ROCINN parameters cloud top height and cloud top albedo, and the total ozone column itself. Figure 13 (top) (Figure 13, bottom) shows normalized histograms for errors induced by a 10% overestimation (underestimation) of cloud fraction. A 10% increase of the cloud fraction induces ~5% decrease for the cloud top albedo and a ~5% increase for the cloud top height. The ROCINN algorithm compensates a possible cloud fraction overestimation by underestimating the cloud top albedo and overestimating the cloud top height. Thus the net effect of combined OCRA/ROCINN uncertainties is to maintain the level of ozone total column error to the ±0.5% level.

7. Concluding Remarks

[81] This paper is the first of two to report on the complete reprocessing of the entire GOME total ozone record using the GOME data processor Version 4.0 implemented in 2004 as part of the ERS-2 Ground Segment at the D-PAF processing facility in DLR Germany. In the first paper, we have given a detailed description of the GDP 4.0

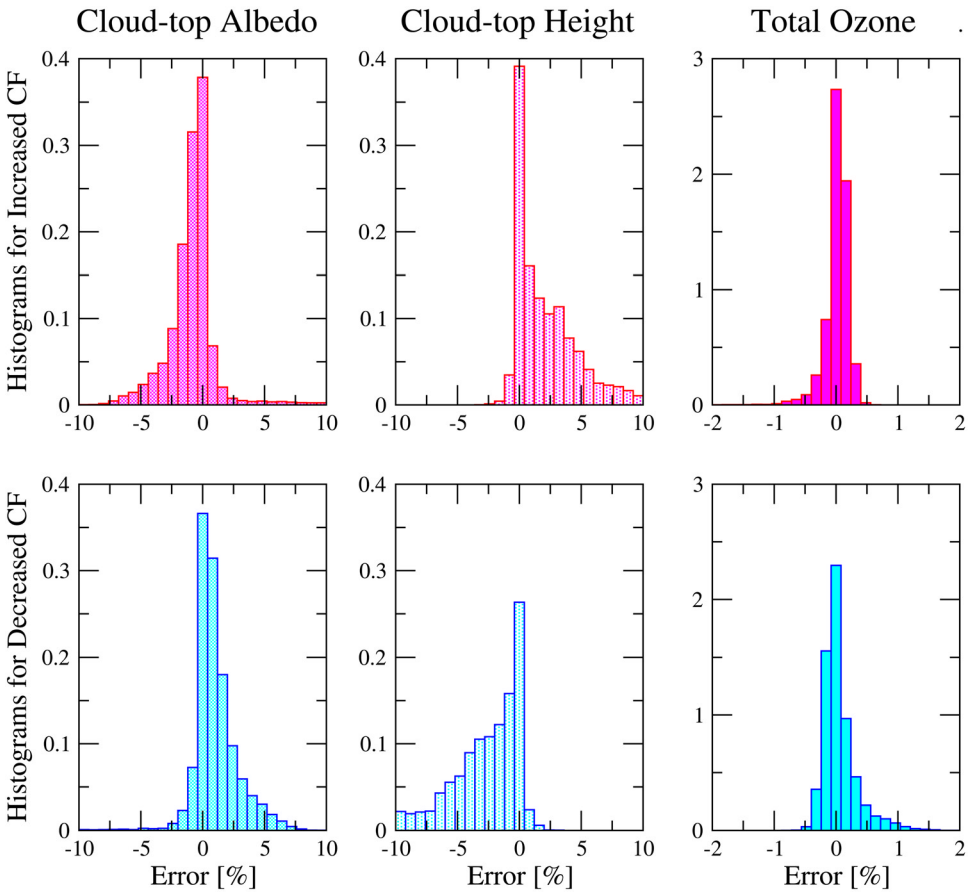

Figure 13. (top) Normalized histograms for errors induced by a 10% overestimate of OCRA's cloud fraction and (bottom) a 10% underestimate of the cloud fraction. Relative errors for cloud (left) top albedo, (middle) cloud top height, and (right) total ozone are shown. A 10% increase in cloud fraction induces a ~5% decrease of the cloud top albedo and a ~5% increase of the cloud top height. The net error on total ozone stays at the 0.5% level.

algorithm. We have discussed the improvements in the DOAS slant column fitting and AMF algorithm components in GDP 4.0 compared with their implementations in the predecessor version GDP 3.0. Iterative AMF computations are done directly with calls to the LIDORT scattering code; the formalism uses the column-classified ozone profile climatology in the TOMS version 8 algorithms. We summarize a new treatment of the molecular Ring effect in GDP 4.0 and its implementation in a DOAS-AMF algorithm, and we discuss new cloud property preprocessing algorithms. The GDP 4.0 algorithm is robust in performance and capable of real-time data turnover in operational execution.

[82] Results from the 10-year reprocessing demonstrate the remarkable stability of the ozone record. The mean amplitude for 10-year comparisons with data from the Hohenpeissenberg Brewer instrument is 0.5%. For viewing conditions with SZA < 80°, the precision of the total ozone column product is better than 2.4% for clear sky scenes, and less than 3.3% for cloudy scenes. For higher SZA up to 88°, the corresponding figures are 4.9% and 5.9%. An extensive validation of the GDP total ozone product [*Balis et al.*, 2006] shows that comparisons with ground based data are often at the 1–1.5% level or better for SZA < 70°, and in polar regions and for scenarios with higher SZA values, discrepancies are up to ±5%. This represents a considerable improvement from the GDP 3.0 record, where validated total ozone results were generally between −2% and 4% of ground-based values for SZA < 70°, and up to 8% for polar and high-SZA scenes.

[83] The GDP 4.0 algorithm will continue to benefit from upgrades in the reference and climatological data set. New column-classified GOME-based ozone profile climatology is currently under construction, derived from 7 years of retrieved profiles obtained from GOME by means of neural network methods [*Müller et al.*, 2003]. Further improvements to the ROCINN algorithm are currently under investigation, with a view to improving look-up tables of radiances by including scattering, polarization and non-Lambertian effects. The GOME LER albedo database and the OCRA cloud-free composite will be updated as more data is processed. Algorithm research is currently focused on the direct fitting of GOME total ozone using classical inversion methods and linearized forward models; this is the GODFIT algorithm [*Van Roozendael et al.*, 2004]. GODFIT has been validated for a subset of the GDP 4.0 validation orbits, and the overall accuracy for this algorithm is comparable to that from GDOAS in GDP 4.0 and also from the

TOGOMI/TOSOMI [*Eskes et al.*, 2005] and WFDOAS [*Coldewey-Egbers et al.*, 2005] algorithms.

[84] The GDP 4.0 total ozone and nitrogen dioxide data from July 1995 was released officially by ESA in December 2004. An algorithm theoretical basis document (ATBD) and a validation report and disclaimer can be found at http://earth.esa.int/services/esa_doc/doc_gom.html#. The reprocessed GOME data record, including historical data, is available to the public at no cost via ftp server using a simple registration procedure through the ERS Help and Order Desk. Further details may be found on the Web (http://wdc.dlr.de/sensors/gome and http://www.oma.be/GOME). Software to handle the GOME data is available at http://www.science-and-technology.nl/beat/.

[85] **Acknowledgments.** Many scientists at a number of institutions in Europe and America have made contributions to the GOME data processing effort. In particular, we would like to thank colleagues from Universität Bremen (Germany), KNMI (Netherlands), Universität Heidelberg (Germany), BIRA-IASB (Belgium), DLR (Germany), SAO (USA), SRON (Netherlands), NASA Goddard (USA), RAL (Great Britain), and AUTH (Greece). We would also like to thank colleagues from the agencies ESA-ESTEC (Netherlands), ESA-ESRIN (Italy), and EUMETSAT (Germany). This work was funded through two ESA contracts: Upgrade of the GOME data processor for Improved Total Ozone Columns, ERSE-ESPR-EOPS-SW-04-0001, and Development of Algorithms for Retrieval of GOME Total Ozone Column, ESRIN contract 16403/02/I-LG. The paper has benefited greatly from three excellent reviews, and we would like to take this opportunity to thank the reviewers for their careful attention to this work. To order GOME products or for further information, please contact EO Help Desk, ESA ESRIN, Via Galileo Galilei, I–00044 Frascati, Italy (phone: +39 06 94180 777; fax: +39 06 94180 272; e-mail: eohelp@esa.int).

References

Aberle, B., W. Balzer, A. von Bargen, E. Hegels, D. Loyola, and R. Spurr (2002), GOME level 0 to 1 algorithms description, *Tech. Note ER-TN-DLR-GO-0022(Issue 5/B)*, Dtsch. Zent. für Luft und Raumfahrt, Oberpfaffenhofen, Germany.

Aliwell, S. R., et al. (2002), Analysis for BrO in zenith-sky spectra: An intercomparison exercise for analysis improvement, *J. Geophys. Res.*, *107*(D14), 4199, doi:10.1029/2001JD000329.

Balis, D., et al. (2006), Ten years of GOME/ERS-2 total ozone data—The new GOME data processor version 4: 2. Ground-based validation and comparisons with TOMS V7/V8(2005), *J. Geophys. Res.*, doi:10.1029/1005JD006376, in press.

Bass, A. M., and R. J. Paur (1985), The ultraviolet cross sections of ozone: I. The measurements, in *Atmospheric Ozone, Proceedings of the Quadrennial Ozone Symposium*, edited by C. S. Zerefos and A. Ghazi, pp. 606–610, Springer, New York.

Bednarz, F. (Ed.) (1995), GOME Global Ozone Monitoring Experiment users manual, *Eur. Space Agency Spec. Publ., SP-1182*.

Berk, A., L. S. Bernstein, and D. C. Robertson (1989), MODTRAN: A moderate resolution model for LOWTRAN-7, *Rep. GL-TR-89–0122*, Geophys. Lab., Hanscomb Air Force Base, Mass.

Bodhaine, B., N. Wood, E. Dutton, and J. Slusser (1999), On Rayleigh optical depth calculations, *J. Atmos. Oceanic Technol.*, *16*, 1854–1861.

Boersma, K. F., H. J. Eskes, and E. J. Brinksma (2004), Error analysis for tropospheric NO_2 retrieval from space, *J. Geophys. Res.*, *109*, D04311, doi:10.1029/2003JD003962.

Bovensmann, H., J. Burrows, M. Buchwitz, J. Frerick, S. Noel, V. Rozanov, K. Chance, and A. Goede (1999), SCIAMACHY: Mission objectives and measurement modes, *J. Atmos. Sci.*, *56*, 127–150.

Bowker, D. E., R. E. Davies, D. L. Myrick, K. Stacy, and W. T. Jones (1985), Spectral Reflectances of natural targets for use in remote sensing studies, *NASA Ref. Publ.*, *1139*.

Burrows, J., A. Dehn, B. Deters, S. Himmelmann, A. Richter, S. Voigt, and J. Orphal (1998), Atmospheric remote-sensing reference data from GOME: Part 1. Temperature-dependent absorption cross-sections of NO2 in the 231–794 nm range, *J. Quant. Spectrosc. Radiat. Transfer*, *60*, 1025–1031.

Burrows, J., et al. (1999a), The Global Ozone Monitoring Experiment (GOME): Mission concept and first scientific results, *J. Atmos. Sci.*, *56*, 151–175.

Burrows, J., A. Richter, A. Dehn, B. Deters, S. Himmelmann, S. Voigt, and J. Orphal (1999b), Atmospheric remote sensing reference data from GOME: Part 2. Temperature-dependent absorption cross-sections of O_3 in the 231–794 nm range, *J. Quant. Spectrosc. Radiat. Transfer*, *61*, 509–517.

Chance, K. (1998), Analysis of BrO measurements from the Global Ozone Monitoring Experiment, *Geophys. Res. Lett.*, *25*, 3335–3338.

Chance, K., and R. Spurr (1997), Ring effect studies: Rayleigh scattering including molecular parameters for rotational Raman scattering, and the Fraunhofer spectrum, *Appl. Opt.*, *36*, 5224–5230.

Chance, K., P. I. Palmer, R. J. D. Spurr, R. V. Martin, T. P. Kurosu, and D. J. Jacob (2000), Satellite observations of formaldehyde over North America from GOME, *Geophys. Res. Lett.*, *27*, 3461–3464.

Coldewey-Egbers, M., M. Weber, L. N. Lamsal, R. de Beek, M. Buchwitz, and J. P. Burrows (2005), Total ozone retrieval from GOME UV spectral data using the weighting function DOAS approach, *Atmos. Chem. Phys.*, *5*, 1015–1025.

De Graaf, M., P. Stammes, O. Torres, and R. Koelemeijer (2005), Absorbing aerosol index: Sensitivity analysis, application to GOME and comparison with TOMS, *J. Geophys. Res.*, *110*, D01201, doi:10.1029/2004JD005178.

Eskes, H. J., R. J. van der A, E. J. Brinksma, J. P. Veefkind, J. F. de Haan, and P. J. M. Valks (2005), Retrieval and validation of ozone columns derived from measurements of SCIAMACHY on Envisat, *Atmos. Chem. Phys. Discuss.*, *5*, 4429–4475.

Fortuin, J. P. F., and H. Kelder (1998), An ozone climatology based on ozonesonde and satellite measurements, *J. Geophys. Res.*, *103*, 31,709–31,734.

Grainger, J. F., and J. Ring (1962), Anomalous Fraunhofer line profiles, *Nature*, *193*, 762.

Hasekamp, O. P., and J. Landgraf (2001), Ozone profile retrieval from backscattered ultraviolet radiances: The inverse problem solved by regularization, *J. Geophys. Res.*, *106*, 8077–8088.

Herman, J. R., and E. A. Celarier (1997), Earth surface reflectivity climatology at 340–380 nm from TOMS data, *J. Geophys. Res.*, *102*, 28,003–28,011.

Hoogen, R., V. V. Rozanov, and J. P. Burrows (1999), Ozone profiles from GOME satellite data: Algorithm description and first validation, *J. Geophys. Res.*, *104*, 8263–8280.

Kneizys, F. X., E. P. Shettle, L. W. Abreu, J. H. Chetwynd, G. P. Anderson, W. O. Gallery, J. E. A. Selby, and S. A. Clough (1988), Users guide to LOWTRAN 7, *Environ. Res. Pap. 1010, Rep. AFGL-TR-88–0177*, Air Force Geophys. Lab., Hanscomb Air Force Base, Mass.

Koelemeijer, R. B. A., P. Stammes, J. W. Hovenier, and J. F. de Haan (2001), A fast method for retrieval of cloud parameters using oxygen A band measurements from the Global Ozone Monitoring Experiment, *J. Geophys. Res.*, *106*, 3475–3490.

Koelemeijer, R. B. A., J. F. de Haan, J. W. Hovenier, and P. Stammes (2003), A database of spectral surface reflectivity in the range 335–772 nm derived from 5.5 years of GOME observations, *J. Geophys. Res.*, *108*(D2), 4070, doi:10.1029/2002JD002429.

Kuze, A., and K. V. Chance (1994), Analysis of cloud top height and cloud coverage from satellites using the O_2 A and B Bands, *J. Geophys. Res.*, *99*, 14,481–14,491.

Lambert, J.-C., M. Van Roozendael, J. Granville, P. Gerard, P. C. Simon, H. Claude, and J. Staehelin (1996), Comparison of the GOME ozone and NO_2 total amounts at mid-latitude with ground-based zenith-sky measurements, in *Atmospheric Ozone: Proceedings of 18th Quadrennial Ozone Symposium, L'Aquila, Italy, 12–21 September 1996*, vol. 1, edited by R. D. Bojkov and G. Visconti, pp. 301–304, Int. Ozone Comm., L'Aquila, Italy.

Lambert, J.-C., M. Van Roozendael, M. De Maziere, P. C. Simon, J.-P. Pommereau, F. Goutail, A. Sarkissian, and J. F. Gleason (1999), Investigation of pole-to-pole performances of spaceborne atmospheric chemistry sensors with the NDSC, *J. Atmos. Sci.*, *56*, 176–193.

Lambert, J.-C., et al. (2000), Combined characterization of GOME and TOMS total ozone measurements from space using ground-based observations from the NDSC, *Adv. Space. Res.*, *26*, 1931–1940.

Lambert, J.-C., et al. (2002), ERS-2 GOME GDP3.0 implementation and validation, edited by J.-C. Lambert, *Tech. Note ERSE-DTEX-EOAD-TN-02–0006*, 138 pp., Eur. Space Agency, Noordwijk, Netherlands.

Liu, X., K. Chance, C. E. Sioris, R. J. D. Spurr, T. P. Kurosu, R. V. Martin, and M. J. Newchurch (2005), Ozone profile and tropospheric ozone retrievals from Global Ozone Monitoring Experiment: Algorithm description and validation, *J. Geophys. Res.*, *110*, D20307, doi:10.1029/2005JD006240.

Livschitz, Y., and D. Loyola (2003), Design document for the GOME-2 universal processor for atmospheric spectrometers, *Doc. SAF/O3M/DLR/DD/001*, German Aerospace Cent., Oberpfaffenhofen.

Loyola, D. (1999), Parameterization of AMFs using artificial neural networks, in *ESAMS'99 - European Symposium on Atmospheric Measurements From Space*, *Rep. ESA WPP-161*, pp. 709–713, Eur. Space Agency, Noordwijk, Netherlands.

Loyola, D. (2000), Cloud retrieval for SCIAMACHY, paper presented at ERS-ENVISAT Symposium, Eur. Space Agency, Gothenburg, Sweden.

Loyola, D. (2004), Automatic cloud analysis from polar-orbiting satellites using neural network and data fusion techniques, in *IGARSS 2004: 2004 IEEE International Geoscience and Remote Sensing Symposium: Proceedings*, vol. 4, pp. 2530–2534, IEEE Press, Piscataway, N. J.

Loyola, D., and T. Ruppert (1998), A new PMD cloud-recognition algorithm for GOME, *Earth Obs. Q.*, *58*, 45–47.

Loyola, D., et al. (1997), Ground segment for ERS-2 GOME data processor, in *3rd Symposium on Space in the Service of Our Environment, Florence, Italy*, *Eur. Space Agency Spec. Publ.*, *SP-414*, 591–597.

Marquard, L. C., T. Wagner, and U. Platt (2000), Improved air mass factor concepts for scattered radiation differential optical absorption spectroscopy of atmospheric species, *J. Geophys. Res.*, *105*, 1315–1327.

Martin, R., et al. (2002), An improved retrieval of tropospheric nitrogen dioxide from GOME, *J. Geophys. Res.*, *107*(D20), 4437, doi:10.1029/2001JD001027.

Matthews, E. (1983), Global vegetation and land use: New high-resolution databases for climate studies, *J. Clim. Appl. Meteorol.*, *22*, 474–487.

Müller, M. D., K. A. Kaifel, M. Weber, S. Tellmann, J. P. Burrows, and D. Loyola (2003), Ozone profile retrieval from Global Ozone Monitoring Experiment (GOME) data using a neural network approach (Neural Network Ozone Retrieval System (NNORSY)), *J. Geophys. Res.*, *108*(D16), 4497, doi:10.1029/2002JD002784.

Munro, R., R. Siddans, W. J. Reburn, and B. Kerridge (1998), Direct measurement of tropospheric ozone from space, *Nature*, *392*, 168–171.

Richter, A., and J. Burrows (2002), Tropospheric NO_2 from GOME measurements, *Adv. Space Res.*, *29*, 1673–1683.

Rothman, L., et al. (2003), The HITRAN molecular spectroscopic database: Edition of 2000 including updates through 2001, *J. Quant. Spectrosc. Radiat. Transfer*, *82*, 5–44.

Sarkissian, A., H. K. Roscoe, D. Fish, M. Van Roozendael, M. Gil, H. B. Chen, P. Wang, J.-P. Pommereau, and J. Lenoble (1995), Ozone and NO_2 air-mass factors for zenith-sky spectrometers: Intercomparison of calculations with different radiative transfer models, *Geophys. Res. Lett.*, *22*, 1113–1116.

Schiffer, R. A., and W. B. Rossow (1983), The international satellite cloud climatology project ISCCP: The first project of the world climate research program, *Bull. Am. Meteorol. Soc.*, *54*, 779–784.

Siddans, R., B. Kerridge, W. J. Reburn, A. Stevens, and R. Munro (1999), Height-resolved ozone retrievals spanning the troposphere and stratosphere from GOME, in *ESAMS '99—European Symposium on Atmospheric Measurements From Space*, *Rep. ESA WPP-161*, pp. 299–305, Eur. Space Agency, Noordwijk, Netherlands.

Slijkhuis, S., A. von Bargen, W. Thomas, and K. Chance (1999), Calculation of under-sampling correction spectra for DOAS spectral fitting, in *ESAMS'99—European Symposium on Atmospheric Measurements From Space*, *Rep. ESA WPP-161*, pp. 563–569, Eur. Space Agency, Noordwijk, Netherlands.

Slijkhuis, S., B. Aberle, and D. Loyola (2004), GOME data processor extraction software user's manual, *Rep. ER-SUM-DLR-GO-0045*, German Aerospace Cent., Oberpfaffenhofen.

Spurr, R. (1999), Improved climatologies and new air mass factor look-up tables for O_3 and NO_2 column retrievals from GOME and SCIAMACHY backscatter measurements, in *ESAMS'99– European Symposium on Atmospheric Measurements From Space*, *Rep. ESA WPP-161*, pp. 277–284, Eur. Space Agency, Noordwijk, Netherlands.

Spurr, R. J. D. (2002), Simultaneous derivation of intensities and weighting functions in a general pseudo-spherical discrete ordinate radiative transfer treatment, *J. Quant. Spectrosc. Radiat. Transfer*, *75*, 129–175.

Spurr, R. (2003), LIDORT V2PLUS: A comprehensive radiative transfer package for nadir viewing spectrometers, remote sensing of clouds and atmosphere, *Proc. SPIE Int. Soc. Opt.*, 3750.

Spurr, R. J. D., T. P. Kurosu, and K. V. Chance (2001), A linearized discrete ordinate radiative transfer model for atmospheric remote sensing retrieval, *J. Quant. Spectrosc. Radiat. Transfer*, *68*, 689–735.

Spurr, R., et al. (2005), GOME level 1–to-2 data processor version 3.0(2005), a major upgrade of the GOME/ERS-2 total ozone retrieval algorithm, *Appl. Opt.*, *44*, 7196–7209.

Stammes, P., P. Levelt, J. de Vries, H. Visser, B. Kruizinga, C. Smorenburg, G. Leppelmeier, and E. Hilsenrath (1999), Scientific requirements and optical design of the Ozone Monitoring Instrument on EOS-CHEM, *Proc. SPIE Int. Soc. Opt. Eng.*, *3750*, 221–232.

Thomas, W., E. Hegels, S. Slijkhuis, R. Spurr, and K. Chance (1998), Detection of biomass burning combustion products in southeast Asia from backscatter data taken by the GOME spectrometer, *Geophys. Res. Lett.*, *25*, 1317–1320.

Thomas, W., T. Erbertseder, T. Ruppert, M. van Roozendael, J. Verdebout, D. Balis, C. Meleti, and C. Zerefos (2005), On the retrieval of volcanic sulfur dioxide emissions from GOME backscatter measurements, *J. Atmos. Chem.*, *50*, 295–320.

Tuinder, O., R. de Winter-Sorkina, and P. Builtjes (2004), Retrieval methods of effective cloud cover for the GOME instrument: An intercomparison, *Atmos. Chem. Phys.*, *4*, 255–273.

van der A, R. J., R. F. van Oss, A. J. M. Piters, J. P. F. Fortuin, Y. J. Meijer, and H. M. Kelder (2002), Ozone profile retrieval from recalibrated GOME data, *J. Geophys. Res.*, *107*(D15), 4239, doi:10.1029/2001JD000696.

van Oss, R. F., R. H. M. Voors, and R. J. D. Spurr (2002), Ozone profile algorithm, in *OMI Algorithm Theoretical Basis Document*, vol. II, *OMI Ozone Products*, edited by P. K. Bhartia, *Rep. ATBD-OMI-02*, version 2.0, pp. 53–76, NASA Goddard Space Flight Cent., Greenbelt, Md.

Van Roozendael, M., and R. J. D. Spurr (2003), GOME direct fitting (GODFIT) validation report, *ERS Exploitation AO/1–4235/02/I-LG*, Eur. Space Agency, Noordwijk, Netherlands.

Van Roozendael, M., V. Soebijanta, C. Fayt, and J.-C. Lambert (2002), Investigation of DOAS issues affecting the accuracy of the GDP version 3.0 total ozone product, in *ERS-2 GOME GDP 3.0 implementation and Delta validation*, edited by J.-C. Lambert, *Rep. ERSE-DTEX-EOAD-TN-02–0006*, pp. 97–129, Eur. Space Res. Inst., Eur. Space Agency, Frascati, Italy.

Van Roozendael, M., J.-C. Lambert, R. J. D. Spurr, and C. Fayt (2004), GOME direct fitting (GODFIT) GDOAS Delta validation report, *ERS Exploitation AO/1–4235/02/I-LG*, Eur. Space Agency, Noordwijk, Netherlands.

Vountas, M., V. V. Rozanov, and J. P. Burrows (1998), Ring effect: Impact of rotational Raman scattering on radiative transfer in Earth's atmosphere, *J. Quant. Spectrosc. Radiat. Transfer*, *60*, 943–961.

Wagner, T., J. Heland, M. Zöger, and U. Platt (2003), A fast H_2O total column density product from GOME—Validation with in-situ aircraft measurements, *Atmos. Chem. Phys.*, *3*, 651–663.

Weber, M., L. N. Lamsal, M. Coldewey-Egbers, K. Bramstedt, and J. P. Burrows (2005), Pole-to-pole validation of GOME WFDOAS total ozone with ground based data, *Atmos. Chem. Phys. Discuss.*, *4*, 6909–6941.

Wellemeyer, C. G., S. L. Taylor, C. J. Seftor, R. D. McPeters, and P. K. Barthia (1997), A correction for total ozone mapping spectrometer profile shape errors at high latitude, *J. Geophys. Res.*, *102*, 9029–9038.

D. Balis, Laboratory of Atmospheric Physics, Department of Physics, Aristotle University of Thessaloniki, Box 149, GR-54124 Thessaloniki, Greece.

C. Fayt, J.-C. Lambert, and M. Van Roozendael, Belgian Institute for Space Aeronomy, 3 Avenue Circulaire, B-1180 Brussels, Belgium.

P. Kenter, Science & Technology BV, Postbus 2608, 2600 AP Delft, Netherlands.

Y. Livschitz, D. Loyola, and P. Valks, IMF, DLR, PO Box 1116, D-82234 Wessling, Germany.

T. Ruppert, DFD, DLR, PO Box 1116, D-82234 Wessling, Germany.

R. Spurr, RT Solutions, Inc., 9 Channing Street, Cambridge, MA 02138, USA. (rtsolutions@verizon.net)

C. Zehner, ESRIN, ESA, Via Galileo Galilei CP.64, I-00044 Frascati, Italy.